Chapter 11
Transcranial Direct Current Stimulation Integration with Magnetic Resonance Imaging, Magnetic Resonance Spectroscopy, Near Infrared Spectroscopy Imaging, and Electroencephalography

Adam J. Woods, Marom Bikson, Kenneth Chelette, Jacek Dmochowski, Anirban Dutta, Zeinab Esmaeilpour, Nigel Gebodh, Michael A. Nitsche, and Charlotte Stagg

A. J. Woods (✉)
Center for Cognitive Aging and Memory (CAM), McKnight Brain Institute, Department of Clinical and Health Psychology, College of Public Health and Health Professions, University of Florida, Gainesville, FL, USA
e-mail: ajwoods@phhp.ufl.edu

M. Bikson
Department of Biomedical Engineering, The City College of New York, New York, NY, USA

K. Chelette
ANT Neuro North America, Philadelphia, PA, USA

J. Dmochowski
Neural Engineering Laboratory, Department of Biomedical Engineering, Grove School of Engineering, The City College of the City University of New York, New York, NY, USA

A. Dutta
Neuroengineering and Informatics for Rehabilitation Laboratory, Jacobs School of Medicine & Biomedical Sciences, Department of Biomedical Engineering, University at Buffalo SUNY, Buffalo, NY, USA

Z. Esmaeilpour · N. Gebodh
Department of Biomedical Engineering, The City College of the City University of New York, New York, NY, USA

M. A. Nitsche
Department of Psychology and Neurosciences, Leibniz Research Centre for Working Environment and Human Factors, Dortmund, Germany

University Medical Hospital Bergmannsheil, Bochum, Germany

C. Stagg
Oxford Centre for fMRI of the Brain, Nuffield Department of Clinical Neurosciences, University of Oxford, Oxford, UK

Oxford Centre for Human Brain Activity, Department of Psychiatry, University of Oxford, Oxford, UK

H. Knotkova et al. (eds.), *Practical Guide to Transcranial Direct Current Stimulation*, https://doi.org/10.1007/978-3-319-95948-1_11

Introduction

Transcranial direct current stimulation (tDCS) is a non-invasive brain stimulation technique that involves application of low intensity direct currents at the scalp for the modulation of central nervous system excitability in humans (Woods et al. 2016). tDCS is an increasingly important tool, being used in a wide range of human neuroscience applications, as well as a potential adjunct therapy for a range of neurological and psychiatric disorders including chronic stroke recovery, depression and migraine. However, despite its obvious promise, the potential of tDCS cannot as yet be fully exploited as there is still a lack of understanding of the neural mechanisms underpinning stimulation. A key methodological advance toward bridging the gap in our understanding of the neural mechanisms of tDCS effects involves integration of tDCS with modern clinical and cognitive neuroscience techniques. This chapter will discuss integration of tDCS with three major neuroscience techniques: magnetic resonance imaging/spectroscopy (MRI/MRS), near infrared spectroscopy (NIRS) imaging, and human electroencephalography (EEG).

MRI provides a high degree of spatial resolution regarding both brain structure and function, with the ability to assess brain-behaviour questions across the entire brain. However, the temporal resolution of magnetic resonance methods is limited. In contrast, EEG provides a high degree of temporal resolution for neural processes, but overall poor spatial resolution. NIRS provides both spatial and temporal resolution for brain activity, but typically only for tissue near the cortical surface. Each method has both strengths and weaknesses regarding the types of hypotheses that can be tested. From an observational perspective, these techniques provide novel insight into the relationship between brain structure/function and behaviour. However, when combined with tDCS, a wide variety of novel questions and hypotheses can be tested. tDCS provides a method for directly intervening on brain tissue, altering the resting membrane potential of stimulated neurons. Thus, integration of tDCS with these methods provides the ability to evaluate not only correlations between brain function and behaviour, but also experimentally manipulate brain activity in stimulated brain regions and assess how these observational relationships between the brain and behaviour change. Thus, integration of tDCS with modern neuroscience methods has the potential to providing greater causal insight into the brain-behaviour relationship in contrast to observational studies using these methods in isolation. In addition, these integrated methods may also provide critical insight for understanding how, where and when stimulation is most effective in the context of tDCS treatment studies (e.g., pain, cognitive aging, dementia, etc.). This information may prove critical in optimizing treatment efficacy and outcome.

The chapter will review the current state of the art in efforts to integrate MRI/MRS, NIRS, and EEG methodologies and discuss technical challenges commonly

faced with integration. In addition, the chapter will give the reader a better understanding of experimental design concerns that should be considered prior to undertaking integration of tDCS with these methods. We will first describe the integration of tDCS with MRI and MRS methods, also covering arterial spin labelling (ASL). We will then turn to integration of tDCS with NIRS. Finally, we will discuss integration with EEG. In each case, careful considerations must be taken to acquire quality data in the presence of tDCS. This chapter will help the reader to understand what considerations must be made, as well as methods for addressing these issues.

Integration with MRI

To date, the neural effects of tDCS have been primarily studied through experiments utilizing transcranial magnetic stimulation (TMS), sometimes in combination with pharmacological agents (Stagg and Nitsche 2011) which have added greatly to our understanding of the local physiological effects of stimulation. However, in recent years, there has been an increasing interest in using advanced neuroimaging techniques to study the effects of tDCS – both in healthy controls and clinical populations. Once technical difficulties are overcome, the combination of tDCS with Magnetic Resonance (MR) provides a powerful tool that allows us to study not only brain regions directly stimulated by tDCS, but unlike most TMS approaches, also how tDCS modulates activity in the rest of the brain.

It is important to note at this point that the neural effects of tDCS are probably dependent, at least to some extent on a number of parameters of the stimulation paradigm, including the duration of stimulation; the site of stimulation; and the electrode configuration used. The majority of studies investigating the mechanistic underpinnings of tDCS using MR approaches have studied the "conventional" electrode placement as first described by Nitsche and Paulus (Nitsche and Paulus 2000), with one 5 × 7 cm electrode over the primary motor cortex (M1) and one 5 × 7 cm electrode over the contralateral supraorbital ridge, with a current of 1–2 mA applied for up to 20 min. This section will therefore focus on studies using these stimulation parameters, important studies using other electrode placements are included where these shed important light on the mechanisms of tDCS.

It is important to note that while some of the findings from studies involving an M1 montage will be applicable to other sites, it cannot be assumed that this is always the case, and therefore the results from these studies should not be assumed to be directly relevant for other stimulation montages. While it is still not clear exactly what facets of neural anatomy have significant effects on tDCS, the distinctive layers in M1and its position on the anterior bank of the large central sulcus, as well as its anatomical connectivity, may well mean that tDCS effects cortical excitability in this region differently to other cortical areas.

MR Approaches

Functional Magnetic Resonance Imaging (fMRI)

Functional magnetic resonance imaging (fMRI) is a versatile and non-invasive tool that has been used for a number of years to study many aspects of neural activity. The first paper to highlight that fMRI can be used to inform our understanding of how tDCS can modulate activity within the brain was published in 2001 by Baudewig et al. (2001b), since when the literature has been rapidly increasing. The majority of the studies discussed here rely on the quantification of the blood oxygen level dependent (BOLD) contrast, the most widely used fMRI technique, although other fMRI techniques are available, of which Arterial Spin Labelling (see later) is perhaps the most relevant in the context of studying the effects of tDCS.

BOLD Functional MRI

The BOLD signal relies on changes in the relative concentrations of deoxygenated haemoglobin (DeoxyHb) and oxygenated haemoglobin (OxyHb) caused by local changes in brain activity, and is therefore an indirect measure of neuronal activity. The BOLD signal is reliant on the magnetic properties of these two compounds. In brief, DeoxyHb contains an iron molecule making it paramagnetic; meaning it has a significant interaction with the applied magnetic field during MRI. By contrast, OxyHb is diamagnetic, so has little effect on the magnetic field. Therefore, if the ratio of OxyHb:DeoxyHb changes within a localized region of tissue, then this can be detected using BOLD fMRI. However, the precise relationship between changes in neuronal activity and a detectable change in the BOLD signal is complex and not yet fully understood (Aroniadou and Keller 1995; Castro-Alamancos et al. 1995; Hess et al. 1996; Logothetis 2008; Trepel and Racine 1998, 2000). FMRI is currently used in two major approaches to study the effects of tDCS either in the presence or absence of a task.

Task-Based fMRI

Task-based fMRI is the classical brain imaging approach, and is a versatile tool that can be used to inform our understanding of how tDCS can modulate activity within the brain while a task is being performed. Task-based fMRI can be done using a number of paradigms, but broadly the BOLD signal from each brain area is compared during task and rest, where the difference in signal reflects changes resulting from changing neural activity in task-based areas of the brain (Woods et al. 2014). This approach usually results in the acquisition of data across the whole brain with a high spatial (in the order of 2–3 mm) and reasonably high temporal resolution.

Resting State fMRI

Functional MRI acquired while the subject is lying in the scanner at rest, and commonly following the instruction "not to think of anything in particular" is an increasingly used method to studying brain connectivity. Without a super-imposed task to perform, the on-going physiological fluctuations in the BOLD signal associated with quiet wakefulness can be recorded. In any given brain region the BOLD signal will vary across time as a function of on-going neural activity. By studying the relationship of the BOLD signal from one brain region to that of others, regions where the time course of fluctuations are highly correlated can be identified, and these regions are said to be "functionally connected". Studies of functional connectivity can be made using a wide array of statistical methods including those utilizing graph theory and independent component analysis (ICA) approaches (for more detail see, for example (Beckmann et al. 2005; Cole et al. 2010; Fornito et al. 2013).

"Resting State Networks" (RSNs) are robust distributed networks identified from ICA that show coordinated and highly reproducible fluctuations in activity between spatially distinct but anatomically closely connected areas while subjects lie at rest (Fox and Raichle 2007; Raichle et al. 2001; Snyder and Raichle 2012). RSNs are being widely investigated due to observed differences during different cognitive and clinical states. They are thought to reflect intrinsic functional architecture in the brain, and separable networks can be identified within resting fMRI data which closely reflect brain regions that are active during task performance (Beckmann et al. 2005; Smith et al. 2009; Stagg and Nitsche 2011). While the physiological underpinnings of changes in RSN connectivity are are still very much the focus of investigation and open to often complex interpretation (Johansen-Berg 2013; Nitsche and Paulus 2000), it is clear that RSNs are highly sensitive to changes in connectivity in a wide range of diseases (Baudewig et al. 2001a; Filippini et al. 2009; Pievani et al. 2011, 2014), and that resting state fMRI is a potentially powerful approach for the study of a wide range of clinical conditions as it removes the confound of task performance (Aroniadou and Keller 1995; Castro-Alamancos et al. 1995; Fornito et al. 2013; Hess et al. 1996; Logothetis 2008; Trepel and Racine 1998, 2000).

Arterial Spin Labelling (ASL)

Although BOLD fMRI is the most common method of assessing neural activity changes during or following tDCS, it has some limitations. BOLD has a relatively high signal-to-noise ratio, meaning that data can be acquired over relatively short timescales, making is highly suitable for studying the effects of non-invasive brain stimulation, the physiological underpinnings of the BOLD effect are complex and currently relatively poorly understood. This may be of particular importance when

studying the effect of tDCS in clinical populations, where changes in blood supply or neurovascular coupling may be expected.

An alternative approach is that of Arterial Spin Labelling (ASL). ASL is a relatively novel fMRI technique that is able to quantify changes in tissue perfusion directly in the brain. It has a much lower signal to noise ratio than BOLD fMRI but has two significant advantages over the BOLD signal: (1) It is primarily sensitive to low-frequency signals and is therefore the ideal modality to detect blood flow changes induced by the minutes-long tDCS protocols commonly used and (2) the physiological basis of the contrast is inherently simpler to understand than BOLD.

Magnetic Resonance Spectroscopy

As well as utilising advances in functional MR Imaging to understand the activity changes induced by tDCS, MR can also be used to investigate how tDCS affects the neurochemicals underpinning these plastic changes via magnetic resonance spectroscopy (MRS); a technique that enables us to detect and quantify concentrations of different metabolites within a volume of tissue.

MRS was first performed in the human brain in 1985 (Beckmann et al. 2005; Bottomley et al. 1985; Cole et al. 2010; Fornito et al. 2013), and since then has been primarily used to investigate metabolic changes in pathological states. MRS measures signals are produced by the behaviour of certain diamagnetic molecules within a magnetic field. While MRI focuses on the variations in signal across space, MRS most commonly examines signals produced from only one volume of tissue. A number of atomic nuclei have diamagnetic properties, including 1H, 31P and 13C MRS, of which 1H MRS is used most widely. The ability of MRS to discriminate between different molecules relies on the fact that the structure of the molecules within which these atoms are bound, and the environment surrounding these molecules, influence the behaviour of the atoms within the magnetic field. MRS focuses on very small differences in the signals produced by the atoms contained within different metabolites within a predetermined volume of interest (VOI) or voxel (a 3 dimensional pixel).

The characteristic peaks and frequencies of many neurochemicals are well described, meaning that the resonances produced from these metabolites can be identified from sample spectra. The amplitudes of the peaks derived from a given metabolite are directly proportional to the concentration of that compound within the target volume of tissue, therefore allowing accurate quantification.

There are a number of limitations to MRS approaches. The most relevant of these relates to the inherently low signal-to-noise of the technique. Signals in MRS are typically summed across a large volume in comparison with other forms of MR imaging (e.g. in the order of 3 cm × 3 cm × 3 cm in 1H MRS compared with 3 mm × 3 mm × 3 mm in MRI); this creates an increase in the signal produced by

given metabolites relative to the background noise. However even summing across a large area, only metabolites present in millimolar concentrations are detectable. Fortunately, many neurochemicals involved in neurotransmission and metabolism are present in concentrations above this threshold, but others (for example Dopamine) are not, making their detection and quantification impossible with current MRS methods.

MRS lacks some of the flexibility of functional imaging – it requires a large number of options to be pre-specified: volumes of interest must be decided in advance; as must the acquisition parameters, which determine which molecule signals can be resolved. Traditionally MRS only allowed spectra to be obtained of one volume of interest at a time, but recent developments, both for MR Spectroscopic Imaging (MRSI) at 3 T and the advent of ultra-high field 7 T MR scanners have demonstrated robust spectra from multiple brain regions simultaneously (e.g. Fox and Raichle 2007; Lemke et al. 2015; Maudsley et al. 2006; Raichle et al. 2001; Snyder and Raichle 2012). This is of particular importance when considering the use of MRS to study the effects of tDCS, where a control VOI, placed in an anatomically distant site, is important to understand the anatomical limits of any described relationships, often requiring an additional experimental session.

Considerations When Combining tDCS and MRI

To date, tDCS has been integrated with functional magnetic resonance imaging (fMRI), both in terms of Blood Oxygen Level Dependent (BOLD) fMRI (Amadi et al. 2014; Antal et al. 2011; Baudewig et al. 2001b; Stagg et al. 2009b) and Arterial Spin Labelling (ASL) (Stagg et al. 2013; Zheng et al. 2011); as well as proton and non-proton MR Spectroscopy (MRS) (Binkofski et al. 2011; Clark et al. 2011; Stagg et al. 2009a).

tDCS may be combined with MR using two approaches. The techniques may be used sequentially, where the stimulation is delivered outside of the scanner with the participant placed in the scanner before and immediately following the stimulation period. Alternatively, stimulation can be delivered within the bore of the scanner (concurrently) either at the same time as collecting MR data, or during rest.

Both approaches have been used successfully in the literature. A concurrent acquisition is often more advantageous due to the logistical and timing issues associated with removing and replacing the participant before subsequent MR data can be collected. Concurrent acquisition also has the advantage that pre- and post-stimulation data can be controlled for reproducibility (in terms of placement for spectroscopy voxels or high-resolution fMRI slices). However, while there are obvious advantages to concurrent stimulation, integration of tDCS to MRI requires multiple extra considerations including MR specific kit, additional setup criteria and potential adverse effects on MR acquisitions which need to be considered when taking this approach.

The following should be seen only as a summary of the most significant risks of the approach, and given the inherent risks of the technique, tDCS should only be used in the scanner environment by trained individuals.

Practical Considerations When Combining tDCS and MR

Prior to the advent of MR compatible tDCS systems, studies were limited to sequential acquisition. This presents logistical and analytical issues for BOLD fMRI and MRS data, most significantly in terms of accurate subject placement and the need to acquire data as soon as possible after stimulation has ceased, although neither of these are insurmountable. However, with the advent of MR-compatible tDCS system it became possible to stimulate subjects in the bore of the magnet. Thus, participants can undergo baseline scans prior to stimulation, simultaneous acquisition of data during stimulation, and/or post-stimulation scanning immediately after stimulation has ceased while remaining in the same position throughout the scan. This has obvious advantages for studies where the reproducibility of the subject is important, for example for MRS voxel placement or high-resolution fMRI. However, integration of the tDCS device into an MRI system is not without complications, and a number of technical aspects need to be considered carefully.

It perhaps goes without saying that when tDCS is integrated with MRI, standard subject safety standards for both MRI and tDCS (for example, no metal on or in the head, no implants susceptible to electrical current or magnetic fields, etc.) should be adhered to. In addition, standard tDCS acquisition considerations including the accurate localization of electrodes, careful preparation and placement of electrodes, and methods to ensure that electrodes, once sited, remain in a stable location on the head remain critical in order to acquire good quality data.

Concurrent tDCS/MRI requires a specialist kit that is MR compatible and rigorously tested. The use of tDCS within the bore of the MR scanner requires the placement of specially designed MRI-compatible (non-ferrous or appropriately shielded) tDCS electrodes with cables passed from the stimulator, through the magnet suite waveguide, and into the magnet bore. The electrodes used should be fitted with high-ohmic (commonly 10 KOhm) resistors to prevent induction of eddy currents within the stimulating leads. It is vital to ensure that electrodes are not in contact with the head coil, or headphones, to prevent electrode displacement and, also, unexpected interactions between the stimulator and the scanner.

Care should also be taken to keep the leads away from the subject to prevent burns and run parallel to the bore without loops to prevent eddy currents. The tDCS stimulator should be kept in the control room as it is not magnet safe and stimulation, as with tDCS outside the scanner, should be monitored closely by a researcher for the entire duration of the stimulation. Careful monitoring of the subject is particularly necessary as the subject is at a distance and, if engaged in a task during stimulation, verbal communication is impossible.

Electrodes should be carefully prepared with high conductance electrical paste (such as that used for EEG) as the saline-soaked sponges which are often used for tDCS applied outside the scanner will dry out over time, making them unsuitable for use in MRI scans that ordinarily last around 60–90 min. This is particularly the case where often a baseline scan or scans lasting tens of minutes are acquired before tDCS is applied. Dry sponges result in poor conductance of the electrical current, which can be uncomfortable or even painful for the participant and might result in skin burning in severe cases. A thick, even, coating ($\geq$3 mm) of paste should be applied to the electrode to provide sufficient distance between the electrode and scalp, ensuring that stimulation is delivered evenly across the electrode.

As with all tDCS experiments, care should be taken to ensure that the electrodes do not move. However, most tDCS electrodes are not visible using standard MRI acquisition, so they electrodes are often marked with oil-capsules to confirm their position on the resulting MR images. The adhesive quality of the paste often assists in maintaining the electrode placement, but also requires additional straps for fully secure placement. The entire montage can be covered by a relatively loose-fitting cap, which has the dual roles of protecting the electrodes from accidental movement during subject placement in the MR and protecting the scanner from the electrode paste.

Data Quality Considerations When Combining tDCS and MR

The constant electrical current which constitutes tDCS interacts with the magnetic field generated by the MR scanner, resulting in warping of the images acquired. This artifact is of critical concern for BOLD fMRI protocols, as it has the potential to result in false positive changes in the BOLD signal. The magnitude and nature of any artefacts are likely to depend on the exact experimental setup and therefore will vary from centre to centre. This variability is reflected by the published studies: one study demonstrated evidence of BOLD signal within the brains of two cadavers during a concurrent tDCS and fMRI protocol (Antal et al. 2014), strongly suggesting that tDCS is capable of inducing significant BOLD signal, although it is worth noting that in most situations the timecourse of this "activation" is likely to be distinct from the task performed and will most likely follow the stimulation period. Another study demonstrated visual evidence of change in EPI field maps, but this was limited to the scalp and cortical tissue near to the electrode site (Holland et al. 2011). Other sites also observe artefacts directly under the electrodes, but these are limited to the scalp and soft tissues (unpublished data, CJS). However, to date, very few studies have provided explicit data on change in the magnetic field in relation to concurrent tDCS/fMRI, in terms, for example, of visible artefacts, change in signal to noise or non-physiological signal change. The contrasting evidence from the literature demonstrates the need for careful consideration of concurrent data and acquisition of appropriate field map data to allay concerns over false positive functional results from perturbation of the magnetic field.

fMRI Studies of tDCS

The relative ease with which resting-state fMRI experiments can be performed and the absence of the confound of task performance has meant a relatively large number of studies utilizing the combination of tDCS and rs-fMRI have been published. A number of studies have demonstrated that tDCS is capable of modulating the resting functional connectivity between a number of brain regions, although to date no clear consensus across the literature has emerged as to the specific pattern of stimulation-induced changes (Amadi et al. 2014; Bachtiar et al. 2015; Polanía et al. 2011a, b, 2012; Sehm et al. 2012, 2013). This lack of agreement between studies as to the effects of tDCS probably reflects the likely sensitivities of different analysis approaches as well as differences in MR acquisition and stimulation parameters, but makes interpretation of the literature as it stands somewhat difficult.

Task-Based Studies in Healthy Controls

Behaviourally, tDCS applied with anode over M1 concurrently with a motor task has been shown to improve performance in a variety of domains, including motor speed and dexterity (Nitsche et al. 2003; Stagg et al. 2011b), and motor learning and adaptation (Boggio et al. 2006; Nitsche et al. 2003; Reis et al. 2009). In prior studies, tDCS under the cathode electrode has been shown to either impair (Stagg et al. 2011b) or to have no effect on learning (Nitsche et al. 2003; Reis et al. 2009) or simple reaction times (Nitsche et al. 2003). A number of studies have employed task-based fMRI to understand not only the activity changes underlying these behavioural effects within the stimulated cortex, but also in more anatomically distant regions.

Baudewig and colleagues initially confirmed the feasibility of combining functional MRI and tDCS (Baudewig et al. 2001a). In this study, the BOLD signal was recorded in a group of six subjects before and after 5 min of tDCS. The authors reported small stimulation-induced changes in activation in the supplementary motor area (SMA), an effect still noticeable 15 min after the end of stimulation.

Since this work, a number of imaging studies in healthy controls have investigated the effects of tDCS on motor-related activity (Antal et al. 2011; Kwon et al. 2008; Lindenberg et al. 2013; Meinzer et al. 2014; Stagg et al. 2009b). Of these, one investigated the effects of a conventional electrode montage (left M1 and the right supraorbital ridge) and a stimulation period of 10 min, on the performance of a simple explicit sequence learning task (Stagg et al. 2009b). The expected increase in activation after stimulation with the anode over M1 compared to sham was observed in the stimulated M1, ipsilateral dorsal premotor cortex (dPMC) and SMA. After stimulation with cathode over M1, an increase in BOLD signal was observed under the stimulating electrode (left M1), as well as in the contralateral (right) M1, dPMC and SMA.

ASL Studies

The first study to combine tDCS with ASL was performed by Zheng and colleagues, which showed an increase in perfusion after short periods of both anode over M1 and cathode over M1 (Zheng et al. 2011). A subsequent ASL study during concurrent tDCS to the left dorsolateral prefrontal cortex (DLPFC) demonstrated an increase in perfusion during and after stimulation with the anode over left DLPFC and a decrease in perfusion during and after stimulation with the cathode over left DLPFC (Stagg et al. 2013), a finding in line with animal models (Wachter et al. 2011). This study also went on to analyse the tDCS-induced changes in perfusion across the whole brain and demonstrated significantly increased perfusion during the anode over DLPFC condition in those areas anatomically connected to the DLPFC (Stagg et al. 2013).

Combining tDCS with MRS

The majority of studies investigating the effects of tDCS on 1H MRS-measured neurochemistry have focused on applying anode or cathode electrodes over M1. Stimulation with anode over M1 leads to a decrease in MRS measured GABA levels in the stimulated area of cortex (Bachtiar et al. 2015; Kim et al. 2014; Stagg et al. 2009a, 2011a). Studies in parietal cortex have demonstrated a concurrent increase in glutamate/glutamine (Clark et al. 2011; Hunter et al. 2015), though this has not been demonstrated in M1 (Stagg et al. 2009c, 2011a). This lack of consistency between studies raises an interesting question about whether the location of brain stimulation alters its effects on neurochemistry, or whether this is a facet of the different MRS approaches used, but it is not possible to draw global conclusions as neither of these parietal cortex studies examined GABA changes.

Integration with NIRS Imaging

Beyond effects on neuronal excitability, after-effects of tDCS on regional cerebral blood flow (rCBF) have been demonstrated (Zheng et al. 2011). Changes in rCBF can be related to the local neuronal activation, which is termed neurovascular coupling (NVC) (Girouard and Iadecola 2006). NVC is defined by neural activity closely related, spatially and temporally, to rCBF. Although the proposition of a correlation between neuronal activity and the increment of vascular supply due to the brain's energy demand increase is a long-standing concept (Roy and Sherrington 1890): "…the brain possesses an intrinsic mechanism by which its vascular supply can be varied locally in correspondence with local variations of functional activity," the exact cellular mechanism of NVC is still elusive (Girouard and Iadecola 2006).

The importance of NVC to the health of the normal brain has been highlighted in a review by Girouard and Iadecola (2006) that suggested it as a therapeutic target in pathologies associated with cerebrovascular dysfunction. Pulgar (2015) has proposed tDCS for improvement of cerebrovascular dysfunction, based on findings showing that it modulates cerebral vasomotor reactivity (VMR), and heart rate variability (Vernieri et al. 2010). Also, tDCS can influence downstream metabolic systems regulated by the brain (Binkofski et al. 2011). However, the effects depend on the tDCS electrode montage, e.g., List et al. (2015) showed with a double-blind crossover within-subject design that 20 min of stimulation did not affect cerebral autoregulation assessed by low-frequency oscillations (LFO) of cerebral blood flow where VMR was measured by transcranial Doppler sonography. Therefore, they hypothesized that the extracephalic return electrode in the study by Vernieri et al. (2010) may have stimulated the brainstem autonomic centers which can be confirmed with the calculations of electric field (and current density) induced by the tDCS montage (Noetscher et al. 2014).

The neurovascular unit (NVU) consists of the endothelium, glia, neurons, pericytes, and the basal lamina where computational models can capture NVU dynamics (Dutta 2015; Huneau et al. 2015). Simple low-dimensional models can describe NVU as a lumped system to relate neural activity with an "energy" variable (analogous to ATP) as output (Chhabria and Chakravarthy, 2016). ATP is required for neuronal metabolic processes like synapto-vescicular recycling and maintenance of the gradient potential (Attwell et al. 2010; Hamel 2006). Specifically, tDCS-evoked increases of neuronal activity might result in aerobic glycolysis (Vaishnavi et al. 2010) and associated lactate surge (Mintun et al. 2004) which can modulate spatiotemporal activity of primary cortical neurons through a receptor-mediated pathway (Bozzo et al. 2013). Besides the role of lactate in energy metabolism, a signaling molecule inducing calcium influx and the expression of long-term plasticity-related genes in neurons has recently been identified (Yang et al. 2014). Also, glial involvement in tDCS-induced plasticity in mouse brain has been shown using calcium imaging (Monai et al. 2016) where a minimum current of ~50 μA (current density, ~2.5 mA/cm^2) at the anode was required to induce cortex-wide calcium surge. However, at lower current intensity of ~14 μA (current density, ~0.7 mA/cm^2), the calcium surge was local at the anode. Such local effects can be due to subthreshold shift of neuronal resting membrane potentials by tDCS that may alter the spontaneous activity with no effects on synaptic plasticity (Stagg and Nitsche 2011). Alterations in spontaneous activity can affect rCBF via various metabolites like K+, adenosine, NO, or CO2 (Dutta 2015). Four kinds of potassium channels, namely ATP-sensitive potassium channels, calcium-activated potassium channels, delayed rectifier potassium channels, and inward rectifier potassium channels play the major role in maintenance of vascular tone of cerebral blood vessels. Via activation of these channels, efflux of K+ causes closure of voltage-dependent calcium channels leading to vascular relaxation (Bonnet et al. 1991; Brayden 1996; Edwards and Weston 1993; Kitazono et al. 1995; Nelson et al. 1990). Also, neuronal nitric oxide synthase (NOS) plays a significant role in maintenance of cerebral blood flow (Attwell et al. 2010). The aftereffects of stimulation following sufficient duration of

stimulation depend on the modulation of both GABAergic and glutamatergic synapses and are calcium-dependent (Giordano et al. 2017; Stagg and Nitsche, 2011) where activation of neuronal NMDA receptors via glutamate causes an influx of calcium that activates NOS and can further increase blood flow (Attwell et al. 2010). At higher current density, glial involvement in tDCS-induced plasticity is possible (Monai et al. 2016) that can be powerful regulators of neuronal spiking, synaptic plasticity and brain blood flow (Bazargani and Attwell, 2016), and are involved in the generation of calcium waves between neighbored neurons via metabotropic glutamate receptors (Leybaert et al. 1998) leading to cortex-wide calcium surge (Monai et al. 2016). Within NVU, glial-cells astrocytes regulate increased local blood-flow during neuronal activation (high energy demand) by secretion of vasoactive substances like NO, and Prostaglandin E2 that are involved in synaptic plasticity (Leybaert et al. 1998; Oomagari et al. 1991). Anatomical connections between the vascular system and astrocytes at the functional level are well known (Mathiisen et al. 2010). Astrocytes express a surface protein required to detect neuronal activation and facilitate the gated efflux of K+ that causes vasodilation (Paulson and Newman 1987). Astrocytic network has extensive connectivity via gap junctions and direct tDCS effects on the astrocytic network (Dutta 2015) will cause widespread changes in the cerebral blood flow, as shown by a recent study (Takai et al. 2016). Moreover, direct effects on the astrocytic network can facilitate neural efficiency by its priming effects on the NVU (Dutta et al. 2015). Stimulation of astrocytes raises calcium in the end-feet that can have a vasoactive effect on parenchymal arterioles. Dilation or constriction depends on the level of calcium (Mulligan and MacVicar 2004). Here, a transition between vasoconstriction and vasodilatation was observed in single vessels by varying the stimulation intensity (Tsytsarev et al. 2011). Indeed, differences of calcium dynamics are proposed to result in different effects of specific tDCS protocols (Stagg and Nitsche 2011) where astrocytic Ca2+/IP3 signaling has been implicated in the metaplasticity changes of the cortex with tDCS (Monai et al. 2016). Our current understanding of glial involvement in tDCS (Monai et al. 2016) and its relation to neuronal function (Bazargani and Attwell 2016) lends to the possibility of bidirectional interactions between neuronal and hemodynamic responses to tDCS (Dutta 2015). This can lead to multi-timescale cross-talk and resulting complex non-linear spatiotemporal dynamics (Jolivet et al. 2015) that may not remain limited to the area immediately under the stimulation electrode (Takai et al. 2016).

The primary purpose of NVU is to maintain homeostasis of the brain's microenvironment (Abbott et al. 2006) where the hemodynamic component of the tDCS response can be captured by functional magnetic resonance imaging (fMRI) as well as functional near-infrared spectroscopy (fNIRS) neuroimaging. MRI can have a high resolution (up to isotropic resolution of 140 μm (Stucht et al. 2015) with full coverage of human brain but with relatively slow sampling rate (e.g., ASL scan taking approximately 3.5 min (Zheng et al. 2011), and MRI suffers from potentially confounding interference from current flow during tDCS (Antal et al. 2014). Therefore, fNIRS is better suited being an optical functional neuroimaging using NIRS technique (Obrig 2014). NIRS can noninvasively and con-

tinuously measure cerebral hemoglobin oxygenation, which is widely used for monitoring of cerebral vascular status under various clinical conditions. The photons in the near-infrared (NIR) spectral range (650–950 nm) are able to penetrate human tissue. NIR wavelengths can be selected such that the change in concentration of oxy-hemoglobin (O2Hb) and deoxy-hemoglobin (HHb) in the brain tissue can be detected. NIR light spectrum between 700 and 900 nm is mostly transparent to skin, tissue, and bone, while O2Hb and HHb are stronger absorbers of this spectrum. Differences in the absorption spectra of O2Hb and HHb enable us to measure relative changes in hemoglobin concentration through the use of light attenuation at multiple wavelengths (Scholkmann et al. 2014). Two or more wavelengths can be selected, with one wavelength above and one below the isobestic point of 810 nm at which HHb and O2Hb have identical absorption coefficients. Using the modified Beer-Lambert Law (mBLL), relative concentration can be calculated as a function of total photon path length. Typically, the light emitter and detector are placed ipsilaterally on the subjects skull so recorded measurements are due to back-scattered (reflected) light following elliptical pathways. NIRS instrumentation works on different measuring principles, e.g., continuous wave (CW) (Scholkmann et al. 2014), frequency domain (FD) (Fantini 2014), and time domain (TD) (Torricelli et al. 2014). Absolute concentration measurements may be possible with more expensive TD and FD techniques (Scholkmann et al. 2014), but quantification is not a crucial factor when one needs to detect a relative change in O2Hb and HHb in cerebral hemodynamic response to tDCS rather than to quantify the hemodynamic response in absolute terms. CW fNIRS signal is strongly contaminated with systemic interference of superficial origin where more expensive TD fNIRS can discriminate between intra- and extra-cerebral signals (Torricelli et al. 2014). Nevertheless, CW fNIRS offers a relatively inexpensive, non-invasive, safe, and portable method of monitoring microvascular hemodynamics in parallel to tDCS in a neurorehabilitation setting. However, CW fNIRS imaging during tDCS requires identification of systemic interference to avoid measuring fNIRS hemodynamic responses that are not due to neurovascular coupling (Tachtsidis and Scholkmann 2016), e.g., by the means of a regression analysis (Kirilina et al. 2012) using short-separation NIRS measurements (Sood et al. 2015) to explicitly sample the extra-cerebral tissue response.

NIRS Probe Development for Imaging of tDCS Responses

The 4 × 1 HD-tDCS montage allows precise targeting of cortical structures (Villamar et al. 2013). Anode centered HD-tDCS increases cortical excitability and is postulated to induce local neuronal and hemodynamic response during focal stimulation (Sood et al. 2016) that can be captured with NIRS-EEG joint imaging, as shown in Fig. 11.1a, b. Freely available SimNIBS software pipeline (Windhoff et al. 2013) was used to develop a subject-specific head model based on MRI data. SimNIBS incorporates FreeSurfer tools (Fischl 2012) to segment the brain and FSL (Jenkinson

et al. 2012) BET/BETsurf tools to segment the rest of the head. Developers of the SimNIBS software pipeline recommend MPRAGE acquisitions with selective water excitation for fat suppression for FreeSurfer tools to work well (http://simnibs.de/version2/mri_sequences). For FSL BET/BETsurf tools, they recommend high bandwidths both for the T1- and T2-weighted images and thin slices with gaps in-between for the T2-weighted images. Therefore, ideally four sets of images should be acquired, two with fat suppression and two without fat suppression, but with high bandwidth and thin slices. The SimNIBS software pipeline (Windhoff et al. 2013) can use the fat-suppressed T1 as input for FreeSurfer, the fat-suppressed T1- and T2-weighted images to reconstruct the inner skull boundary, and the normal T1- and T2-weighted images to reconstruct the outer skull boundary and the skin surface with FSL (Jenkinson et al. 2012) BET/BETsurft tools. This software pipeline was applied on the Colin27 average brain, which is based on 27 times on an individual, and linear registration of the images to create an average with high SNR and structure definition (Holmes et al. 2015). The tetrahedral head meshes from the Colin27 average brain MRI data were generated using the 'mri2mesh' tool in the SimNIBS software pipeline (Windhoff et al. 2013). The tDCS electrode positions in the SimNIBS software pipeline was defined using MNI coordinates of 10–20 scalp positions given by Okamoto et al. (2004) for the finite element analysis (FEA) using GetDP – a freely available finite element solver (http://getdp.info/). The FEA model used electrostatic volume conductor physics with default (in SimNIBS) material conductivities (in S/m): white matter = 0.126; gray matter = 0.275; CSF = 1.654; bone = 0.01; scalp = 0.465; spongy bone = 0.025; compact bone = 0.008; eye balls = 0.5; eye region = 0.25. The electric field magnitude can be used (Datta et al. 2011) to determine tDCS-affected brain areas as shown in Fig. 11.1c.

The open-source software package AtlasViewer (Aasted et al. 2015) was used to design NIRS probes to cover tDCS-affected (based on electric field magnitude (Datta et al. 2011)) brain areas using NIR sources and detectors. AtlasViewer provides tools for spatial registration, probe sensitivity computation, and reconstruction of images. The NIRS forward model (and probe sensitivity) can be computed by the Monte-Carlo photon transport software, 'tMCimg', available in the AtlasViewer package that computes the probabilistic path of photons from the optode source located at the scalp through the head model tissues to the re-emission at the scalp located optode detectors. Colin27 head model (Holmes et al. 2015) with the International 10–20 system as the reference points for the NIRS probe design. AtlasViewer also provides 'iso2mesh' – an image-based 3D surface and volumetric mesh generator comparable to 'mri2mesh' tool in the SimNIBS software pipeline (Windhoff et al. 2013) – to generate individual MRI-based head models. The AtlasViewer package allows a probe to be designed, amended, and assessed prior to probe fabrication (Aasted et al. 2015). Increasing the source-detector (SD) separation past 2 cm monotonically increases sensitivity to brain tissue; diminishing returns appear to begin at around 4–5 cm (Strangman et al. 2013). The probe sensitivity can be found using the Monte-Carlo (MC) photon transport software 'tMCimg' (Boas et al. 2002) available in the AtlasViewer package. Initial rapid assessment of the probe placement and sensitivity was performed with 1e6 photons and more accu-

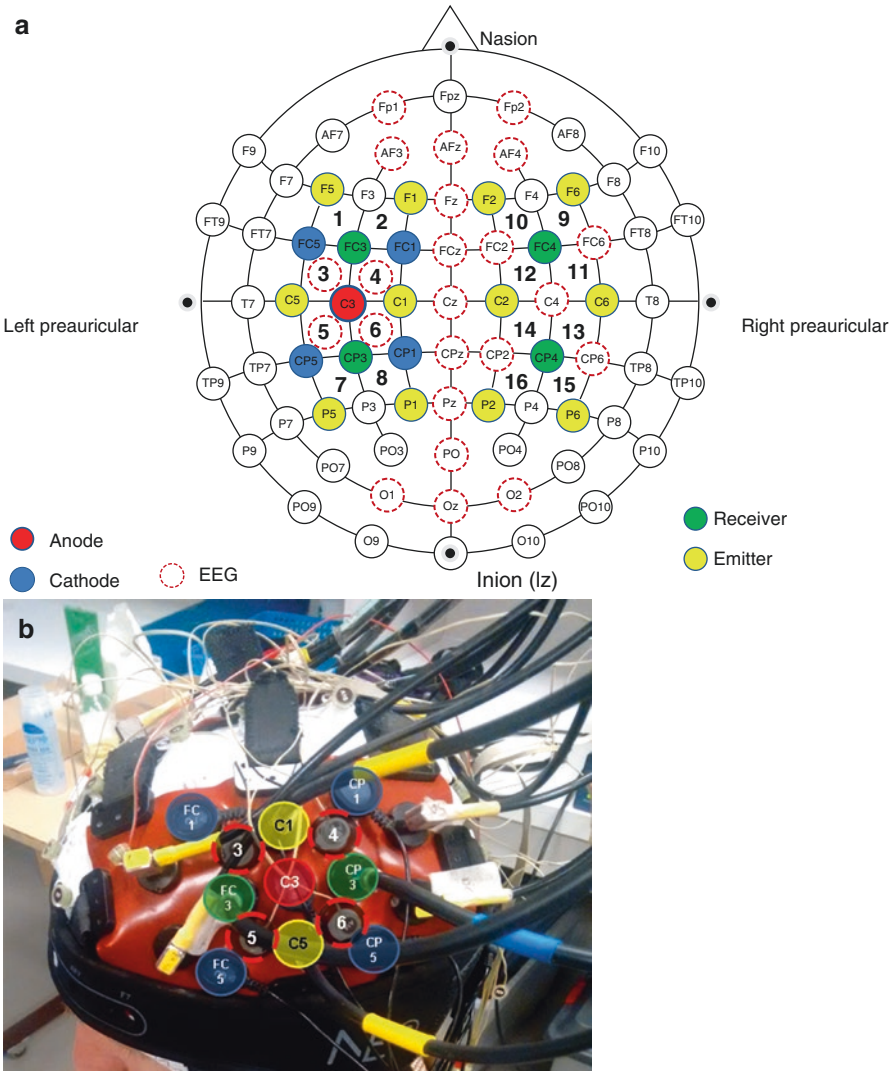

Fig. 11.1 (**a**) An illustrative NIRS-EEG/HD-tDCS montage with NIRS channels, 1–16, according to the standard EEG 10–10 at the ipsilateral and contralateral sensorimotor areas (**b**) The experimental set-up of the HD-tDCS electrodes and local NIRS-EEG channels, 3–6, (**c**) Electric field magnitude due to HD-tDCS in the gray matter surface, (**d**) Sensitivity distribution of NIRS probe at gray matter surface. (Pictures adapted from Sood et al. (2016) with permission)

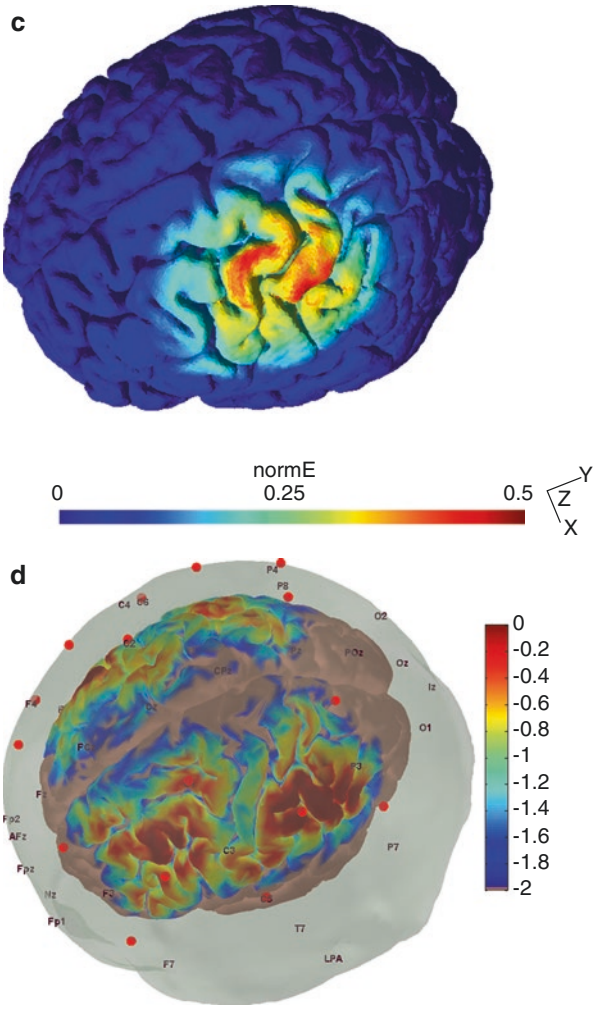

Fig. 11.1 (continued)

rate results were obtained with 1e8 photons to evaluate the final probe design. This time-consuming MC simulation generates the forward matrix that represents the spatial sensitivity profile of each measurement channel to cortical absorption changes. A graphical processor unit can substantially speed up the simulation by more than 100× using mesh-based MC simulation (Fang 2010). The NIRS forward model was identified for the head volume where AtlasViewer projects the volumetric sensitivity in the gray matter onto the surface of the pial matter and implements the AAL atlas (Tzourio-Mazoyer et al. 2002) for localizing the brain region of interest. In fact, NIRS signals in adult humans are strongly biased towards the outermost 1–1.5 cm of the intracranial space (Strangman et al. 2013). Registration of this head model to a subject can be achieved using affine transformation in the AtlasViewer

with fiducials 3D digitized at Nz, Iz, Cz, right and left preauricular points. It is also essential to incorporate optical properties representing heterogeneously lesioned individual brains to build realistic individual head models, especially, for the reconstruction of images of the measured brain activation patterns in stroke survivors.

Preliminary Results

The set-up of the HD-tDCS electrodes and NIRS optodes was formed on the surface of the skull according to the standard used EEG 10–20 (Jasper 1958) at the ipsilateral and contralateral primary sensorimotor cortex (SMC), as shown in Fig. 11.1a, b. The HD-tDCS (Starstim®, Neuroelectrics NE, Barcelona) cathodes were placed on FC1, FC5, CP5 and CP1 with the anode in the center, C3, in a 4 × 1 ring configuration (Fig. 11.1a). The corresponding electric field magnitude at the gray matter surface is shown in Fig. 11.1c. Measurements of hemodynamic changes were made from 16-channel CW NIRS system (Oxymon MkIII, Artinis, Netherlands) at a sampling frequency of 10 Hz. Pathlength Differential Factor was calculated based on the age of the subject in order to know the variations in concentration of O2Hb and HHb (Delpy et al. 1989). The receiver-transmitter distance of 3 cm was chosen based on computational modeling; the respective measurement sensitivity distribution of the NIRS probe at the gray matter surface is shown in Fig. 11.1d. The receivers (Rx) were placed on FC3 and CP3 for the left hemisphere and FC4 and CP4 for the right hemisphere (Fig. 11.1a). Transmitters (Tx) were placed diagonally, i.e., at P1, P5, C1, C5, F5 and F1 for the left hemisphere and at P6, P2, C6, C2, F2 and F6 for the right hemisphere. These Rx and Tx fibres were held in place with a plastic ring on a 1 mm thick silicone-based band and the bands were held together with Velcro® tape (see Fig. 11.1b). The experiment was divided into three sessions: 10 min before (pre), at 10 min during ("online"), and 3 min after ("offline") anode centered HD-tDCS of the SMC (2 mA: 20 min), the subject performed a self initiated simple finger sequence (SFS) task with their right and left hand in an alternating block design (30-s task and 30-s rest, repeated 5 times). The fNIRS results showed that anodal HD-tDCS induced a significant reduction in bilateral SMC activation (i.e., smaller decrease in HHb) for a similar SFS frequency (i.e., motor output) (Muthalib et al. 2016) that is shown for NIRS channels 4 and 12 (left and right SMC respectively) in Fig. 11.2a. Muthalib and colleagues (2016) postulated that anodal HD-tDCS induced a "greater efficiency" of neuronal transmission in the bilateral SMC to perform the same SFS task where "greater efficiency" can be related to anodal HD-tDCS "priming" the NVU with evoked hemodynamic response (Guhathakurta and Dutta 2016). Indeed, the resting state fNIRS data showed focal hemodynamic responses as a correlate of the electrical field distribution (see Fig. 11.1c) in the stimulated hemisphere during HD-tDCS (Muthalib et al. 2016). Figure 11.2b shows that online HD-tDCS at rest induced a gradual increase in the concentration of O2Hb (red line) at the left hemisphere peaking after 5 min at the fNIRS channels located adjacent to the 4 × 1 HD-tDCS electrode montage (e.g.,

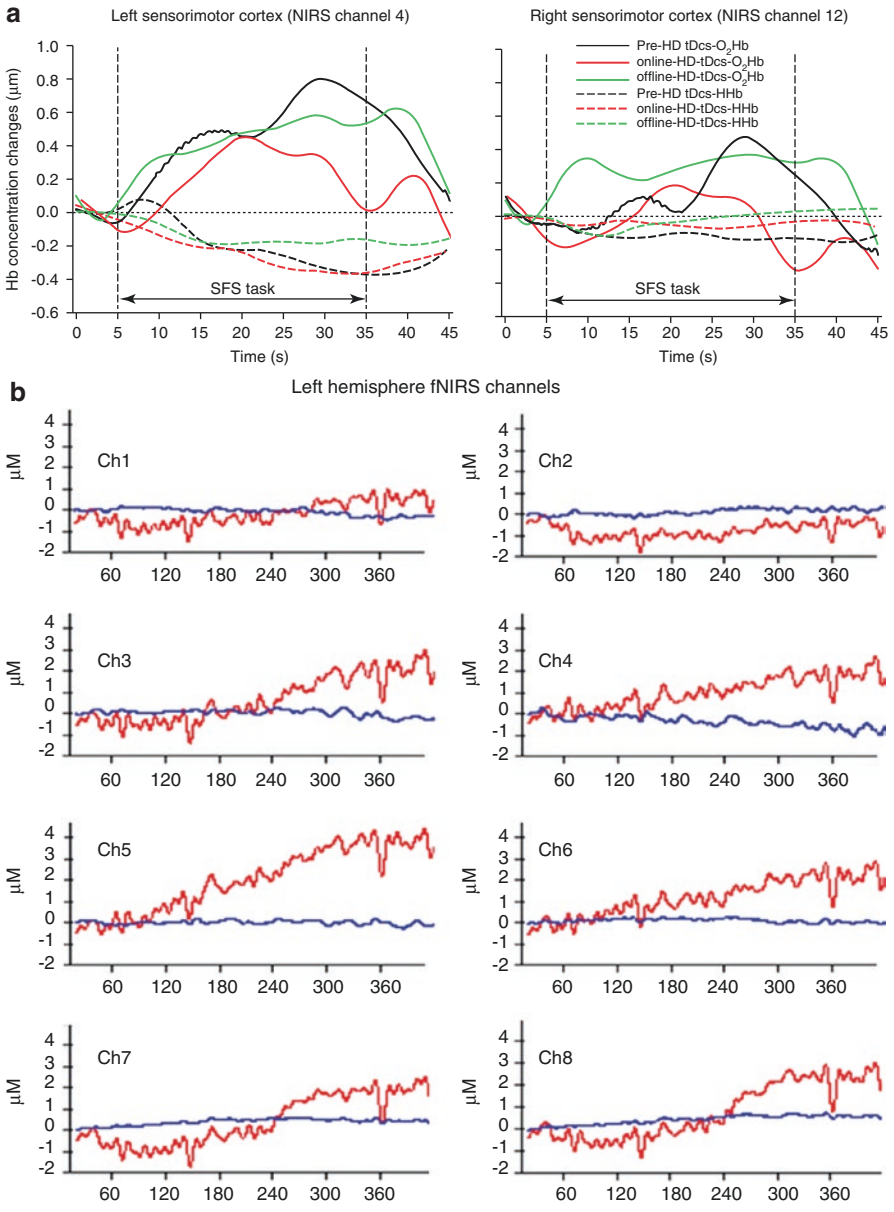

Fig. 11.2 Illustrative fNIRS result in healthy humans. (Adapted from Muthalib et al. (2016), (Muthalib et al. 2017)). (**a**) fNIRS changes of left SMC (left panel: channel 4) and right SMC (right panel: channel 12) during the right hand simple finger sequence (SFS) task before "Pre", during "Online" and after "Offline" anode centered HD-tDCS. (**b**) Online HD-tDCS at rest induced a gradual increase in the concentration O2Hb (red line peaking after 5 min, x-axis shows the number of the datapoint sampled at 10 Hz) in the left hemisphere fNIRS channels (3, 4, 5, 6) located adjacent to the 4 × 1 HD-tDCS electrode montage. The concentration of HHB (blue line) did not show a significant change during HD-tDCS

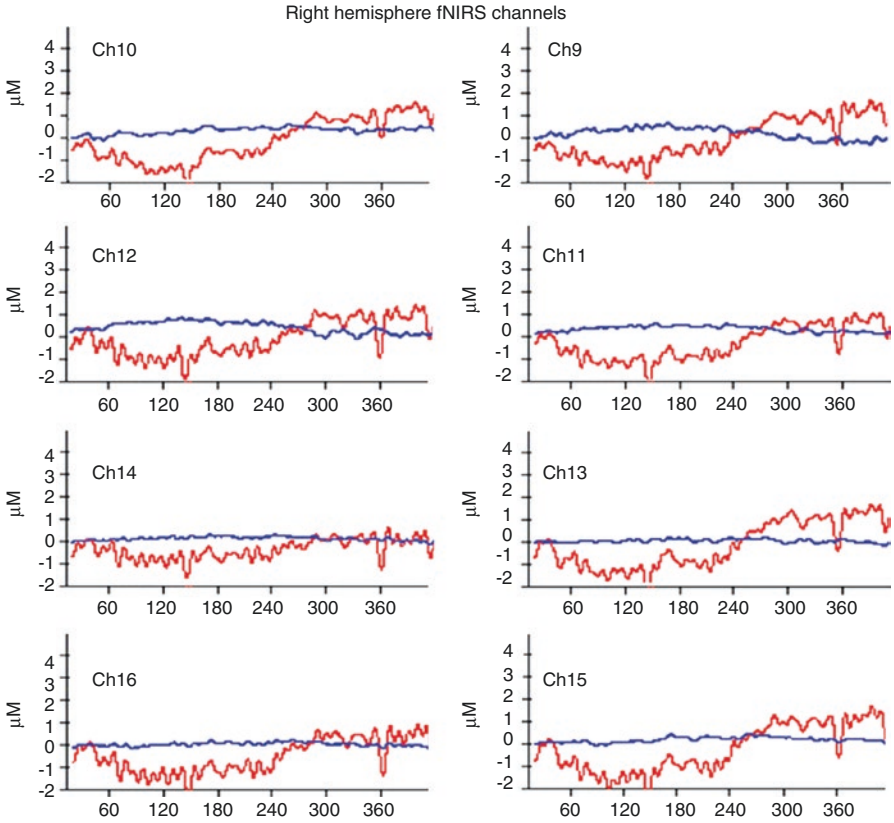

Fig. 11.2 (continued)

channels 3, 4, 5, 6). Also, online HD-tDCS at rest induced a decrease in the concentration of O2Hb (red line) at the right (contralateral) hemisphere (e.g., channels 9–15) peaking after 2 min which may be related to inter-hemispheric inhibition. However, the concentration of HHB (blue line) did not show a significant change during HD-tDCS where tDCS can have direct effects on glial cells (Monai et al. 2016) and smooth muscles of blood vessels (Pulgar 2015) without affecting oxygen utilization leading to alterations in rCBF (and O2HB). Therefore, an analysis of the resting-state NVC was conducted based on local NIRS-EEG channels adjacent to the 4 × 1 HD-tDCS electrode montage (i.e., channels 3, 4, 5, 6). An autoregressive (ARX) model was developed to track the transient coupling relation between log (base-10) transformed EEG band-power (0.5–11.25 Hz) and NIRS O2Hb signal in the low frequency (≤0.1 Hz) range (Sood et al. 2016), as shown in Fig. 11.3. This transient coupling fluctuated between in-phase and out-of-phase during anodal HD-tDCS which may be due to the dynamics within NVU. A stroke case-series demonstrated an impaired NVC functionality during anodal tDCS in chronic (>6 months) ischemic stroke survivors (Dutta et al. 2015) that revealed the lesioned hemisphere with impaired circulation (Jindal et al. 2015). Therefore, we postulate

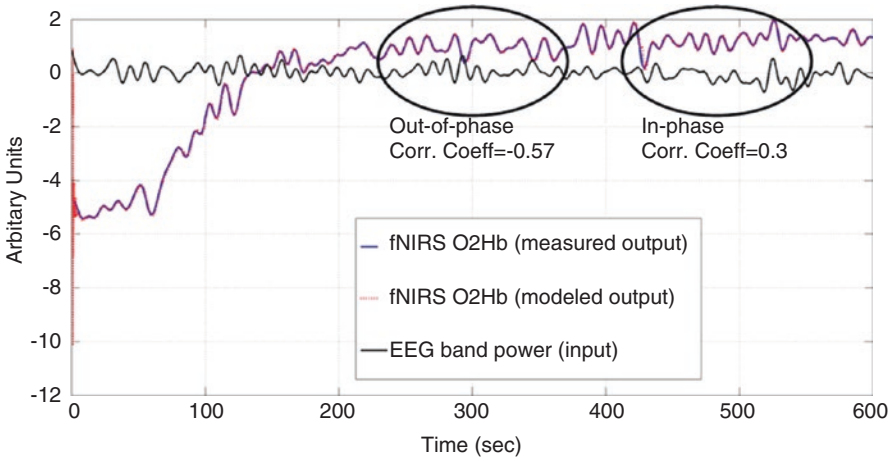

Fig. 11.3 Transient coupling in the low frequency (≤0.1 Hz) range between the electrophysiological (EEG band power within 0.5–11.25 Hz) and the hemodynamic (fNIRS O2Hb) signals representing resting-state spontaneous brain activation during anodal HD-tDCS in healthy humans. (Picture adapted from Sood et al. (2016) with permission)

that portable NIRS-EEG joint imaging of tDCS responses incorporated into brain computer interfaces may be used to identify, assess, and customize dosing of tDCS in cerebrovascular diseases (Dutta 2015).

Integration with EEG

Recent technological advances in the field of EEG and tDCS have allowed for increasingly seamless integration of tDCS and EEG. Combining non-invasive brain stimulation with imaging, especially concurrent online integration, provides objective outcome measures and allows for optimization of the interventions (Baudewig et al. 2001a; Hunter et al. 2013; Komssi et al. 2002). These optimizations can be done using the concept of reciprocity, which suggests that EEG electrical recordings can be inverted to guide electrical stimulation (tDCS) to specific targets within the brain (Cancelli et al. 2016; Fernández-Corazza et al. 2016; Wagner et al. 2016). Similar to other integrated modalities though, the integration of EEG and tDCS does come with some limitations. These can include the type of integration, hardware limitations, as well as several types of artifacts that can occur with integration.

Both EEG and tDCS (Minhas et al. 2010) use conductive interfaces between electrodes and scalp across the head, are portable and low-cost (Charvet et al. 2015), and have broad applications spanning the cognitive and neuropsychiatric domains (Al-Kaysi et al. 2016; Brunoni et al. 2012; Buch et al. 2017). In the case of EEG, electrolyte gel is used between the scalp and recording electrodes, whereas with tDCS saline soaked sponges or electrolyte gel can be used, specifically in

HD-tDCS. The use of HD-tDCS when combined with EEG is advantageous compared to traditional tDCS, due to its increased focality, small area required to apply stimulation as well as its gel interface with the scalp, which is similar that of EEG. Analogous to EEG, with HD-tDCS small stimulation electrodes holders are used to hold externally applied stimulating electrodes, alternatively these cups can incorporate both stimulation and recording electrode options. With the integration of EEG with tDCS protocols, high resolution real time scalp voltage monitoring can be achieved as well as voltage dynamics and frequency shifts prior to, during, and after tDCS. These features, combined with the perception that tDCS produces only DC artifacts in the EEG that are readily filtered, have encouraged human trials of concurrent (online) EEG recording during tDCS (Cunillera et al. 2015; Faehling and Plewnia 2016; Faria et al. 2012; Mancini et al. 2015; Mangia et al. 2014; Roy et al. 2014).

Previous studies that have reported on concurrent tDCS and EEG have used signal processing of varying complexity to remove what are presumed "non-physiologic stimulation artifacts" – namely artifacts that arise from non-ideal stimulation and recording amplifier performance (Cunillera et al. 2015; Faehling and Plewnia 2016; Faria et al. 2012; Mancini et al. 2015; Mangia et al. 2014; Roy et al. 2014). Studies reporting effects of tDCS on EEG have made varied assumptions about the nature of the stimulation artifact such as: the artifact is narrowband in the frequency domain (DC at 0 Hz), allowing for simple high-pass filtering; or the artifact is time invariant, supporting stationary artifact removal techniques (e.g. ICA); the artifact is montage independent, supporting the use of control tDCS montages (i.e. montage/polarity/current specific); and/or the artifacts do not outlast stimulation, supporting pre/post (offline) comparisons without need for corrections. In light of new and emerging evidence though, these assumptions warrant further testing (Noury et al. 2016).

EEG Integration Approaches: Practical Aspects

With the integration of EEG and tDCS technologies several approaches can be taken. These approaches can be structured upon practical limitations with experimental design, hardware limitations, or regions of interest on the scalp. Experimental design is a key component that should be considered when designing EEG –tDCS protocols. This can influence the type of hardware used as well as quality of data acquired. For example, if comparisons of offline (no stimulation) and online (stimulation) EEG are to be compared, understanding what type of baseline measures to compare to and when to acquire proper baseline measures would be important. Improper experimental designs including inadequate tDCS washout periods, missing study arms, etc. can introduce detrimental confounds that can detract from meaningful study outcomes and should be avoided. Specific regions of interest on the scalp (i.e. standard sites C3 commonly associated with motor cortex stimulation) may influence the selected EEG electrode density and placement, relative to stimulation sites. It can also dictate the number of head caps used (i.e. one solely for acquiring EEG and one solely for applying stimulation).

Hardware limitations, including the lack of bandwidth or encoding bit depth to record large voltages produced by stimulation, can greatly influence the types of EEG amplifiers used. Amplifiers that cannot accommodate large voltages produced during stimulation can produce nonlinear artifacts when voltages approach the limit of the amplifier's dynamic range. When voltages go beyond the dynamic range of the amplifier non-recoverable saturation occurs, leaving unusable EEG data.

Offline EEG-tDCS

In cases where EEG data during stimulation is not required (or "offline" stimulation) the hardware options are to utilize (1) a single cap with overlapping stimulation and acquisition sites where EEG data acquisition sites are shared with stimulation sites; (2) a single cap with non-overlapping stimulation and acquisition sites where EEG data acquisition sites are interleaved with stimulation sites; or (3) two caps, one for EEG data acquisition with designated EEG electrode positioning and one for HD-tDCS with designated sites for delivering stimulation. With a single cap containing overlapping sites, stimulation sites can be digitally selected and changed from recording to stimulation sites over the course of an experiment. When utilizing a single cap with non-overlapping, interleaved stimulation sites; the option of stimulation at specific data acquisition sites is not available; instead stimulation is delivered to neighboring sites. For example, with an M1SO (motor to contralateral supraorbital) stimulation montage, data can be acquired over the motor cortex from standard site C3 and stimulation can be delivered at standard site C5 (centimeters away from C3) with a contralateral supraorbital return electrode at F8. Utilizing two different caps, involves acquiring data then swapping caps to one that holds stimulation sites then applying stimulation (or vice versa). In this case, if data acquisition and stimulation are done in close temporal proximity to each other, technical issues like gel smearing can arise. This smearing of gel can lead to electrical bridging with EEG data acquisition or current shunting with stimulation and is typically not recommended.

Online EEG-tDCS

If EEG data acquisition during stimulation (or "online" stimulation) is of interest and amplifier bandwidth can accommodate large voltages, then several options, similar to offline stimulation, are available with the use of a single cap. Single or integrated caps can have (1) overlapping stimulation and acquisition sites where at each scalp location electrodes can acquire EEG data or be used to deliver stimulation; or (2) non-overlapping stimulation and acquisition sites where there are sites dedicated solely to data acquisition and additional interleaved scalp locations dedicated to stimulation

(Fig. 11.4a); or (3) selectively removed acquisition sites. When using a cap with overlapping sites, locations for stimulation and data acquisition can be digitally selected and EEG data can be derived from the same points of stimulation during the stimulation. When utilizing online stimulation with non-overlapping sites, acquired data are in close proximity (centimeters away) to stimulation sites but do not overlap with them. With selective removal of acquisition sites, selected EEG recording sites are mechanically removed at some point over the course of an experiment and replaced with stimulating electrodes. They can either be removed during the course of both data acquisition and stimulation or just over the course of stimulation.

Stimulation Device Selection

When designing stimulation protocol, the choice of stimulation device is of great importance. With tDCS, devices that specifically deliver a direct current should be used. Ideally devices that adhere to circuit architectures that utilize current controlled, current sources should be utilized for DC delivery. In many cases, studies performing tDCS have resorted to utilizing iontophoresis devices, which in essence do deliver an averaged desired DC output, but have voltage outputs that are oscillatory. When acquiring online stimulation EEG data with devices such as iontophoresis devices, large oscillatory voltage artifacts can be introduced in acquired EEG data (Fig. 11.5a). These oscillating artifacts can be difficult to attenuate in post processing and can significantly decimate signal quality. For these reasons stimulation devices should be tested to ensure they deliver a stable DC, prior to incorporating them into integrated online stimulation and EEG protocols (see also section "Inherent Stimulator Artifacts").

Characteristics of the DC Voltage

During HD-tDCS, the application of an external direct current strongly influences the recorded voltages at all EEG electrodes (Fig. 11.4b–e). Across protocols (application routines, montages, currents), the largest deviations in voltage track the applied current, increasing to a value during the tDCS ramp up, generally maintaining the value (the "DC offset") during the sustained current phase, and decreasing along with the tDCS ramp down (Fig. 11.5a). The largest positive and negative voltage deviations are observed near the anode and cathode, respectively. These polarity specific offsets indicate that DC offset is montage specific. This indicates that the EEG voltage profile for an M1SO stimulation montage will be different from that of a Bifrontal stimulation montage. Applying 2 mA of current during tDCS produces a DC offset that is up to 1000 fold larger than baseline neural EEG signals (Fig. 11.5a). This large voltage offset is also consistent across all different types of stimulation devices that deliver a DC.

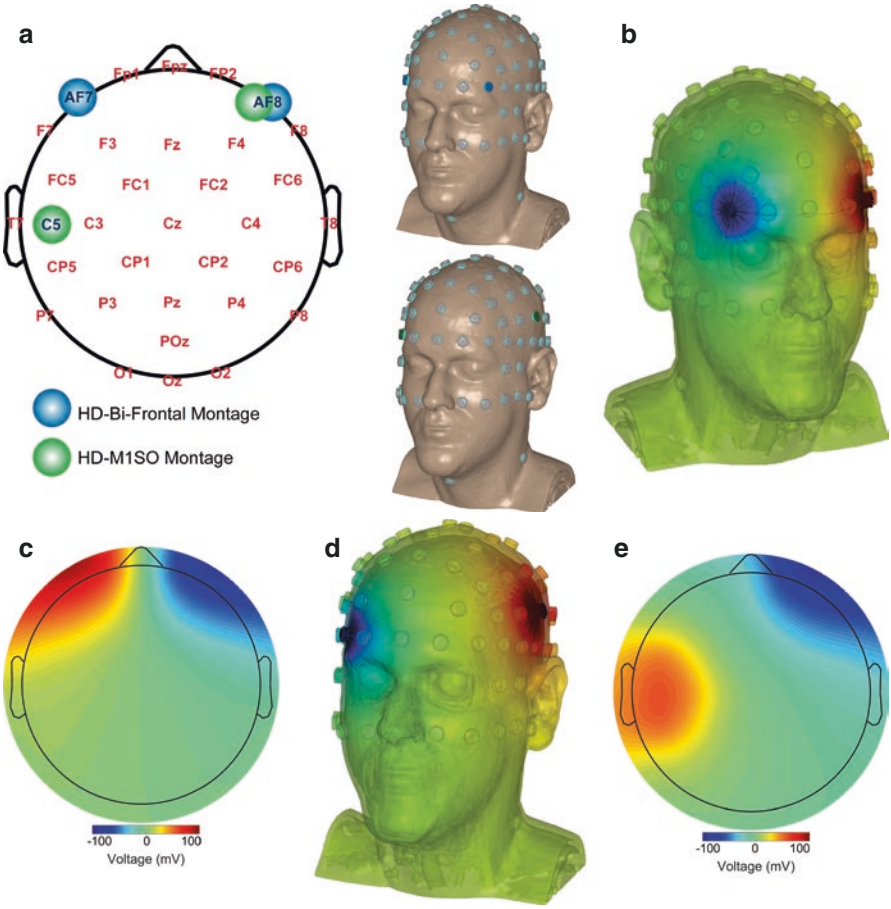

Fig. 11.4 (**a**) EEG cap layout with the locations of the integrated stimulation sites indicated at sites AF7, AF8, and C5. The HD-Bifrontal stimulation montage is demonstrated (blue pairs) where electrodes are placed over standard sites AF7 and AF8. The HD-M1SO montage is demonstrated (green pairs) where electrodes are placed over standard sites AF8 and C5. In both cases polarities can be interchanged within each montage. MRI derived head model indicating scalp locations of stimulating electrodes for HD-Bifrontal stimulation (top, blue disks), HD-M1SO stimulation (bottom, green disks), and some EEG recording electrodes (gray disks). (**b**) Skin voltage distribution predicted by computational models for 2 mA of HD-Bifrontal stimulation where the anode is placed at AF8 and the cathode is placed at AF7. Flux lines (black) indicate direction of current flow across the skin, with maximal voltages near the anode and cathode as well as in frontal EEG electrodes. (**c**) Topographic voltage distribution for 2 mA of HD-Bifrontal stimulation from model predictions. Model scalp voltages were sampled at EEG recording sites for HD-Bifrontal stimulation. (**d**) Skin voltage distribution predicted by computational models for HD-M1SO stimulation where the anode is placed at C5 and the cathode is placed at AF8. Flux lines (black) indicate direction of current flow across the skin, with maximal voltages near the anode and cathode as well as in frontal and left parietal EEG electrodes. (**e**) Topographic voltage distribution for HD-M1SO stimulation from model predictions. Model scalp voltages were sampled at EEG recording sites for HD-M1SO stimulation. With both montages, colorbars indicate voltages for both computational models' skin voltage and scalp topographic distributions

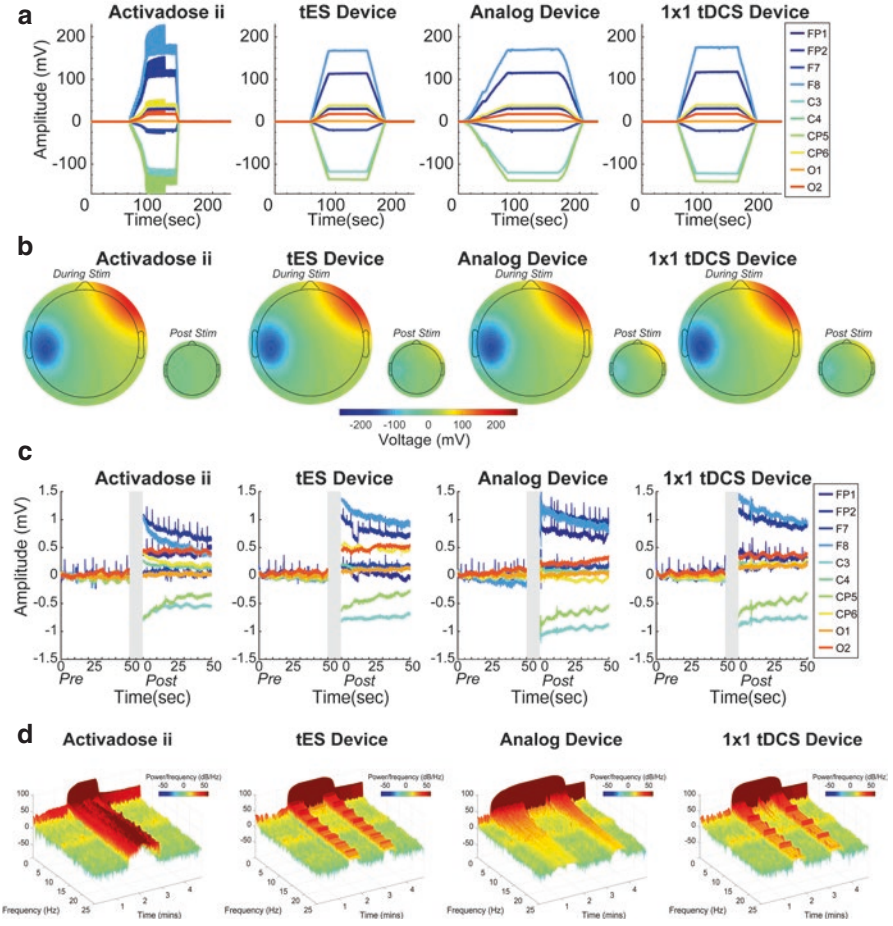

Fig. 11.5 (**a**) Voltage over time across different stimulation devices. The largest voltage offsets or DC voltage is seen at electrodes closest to the stimulation sites (anode: AF8, cathode: C5). The linear ramp-up and ramp-down periods can also be observed at the beginning and end of the stimulation period. (**b**) Mean voltage topographies across stimulation devices where the largest voltage negativity is observed near the cathode (C5) and the largest voltage positivity is observed near the anode (AF8). During the post stimulation period mean voltage topographies show the presence of residual scalp voltage across devices. The spatial distribution of the post stimulation voltage topographies is identical those during stimulation. (**c**) Post stimulation, electrodes exhibit a decay in voltage. Electrodes that are closest to the stimulation sites show the largest residual voltage after stimulation ends. (**d**) Spectrograms over time show the broadband distortion produced during the ramp-up and ramp-down periods. They also show the low-frequency spectral density offset produced during stimulation as well as post stimulation. Physiologically related frequency bands can be seen between 8 and 12 Hz across the pre, during, and post stimulation periods. (**e**) Across devices, the frequency distribution across electrodes differed. Electrodes near the anode show larger power offsets than those near the cathode at lower frequencies (0–10 Hz). (**f**) Compared to baseline conditions electrodes near the cathode (C5) show pronounced peaks between 1 and 1.2 Hz

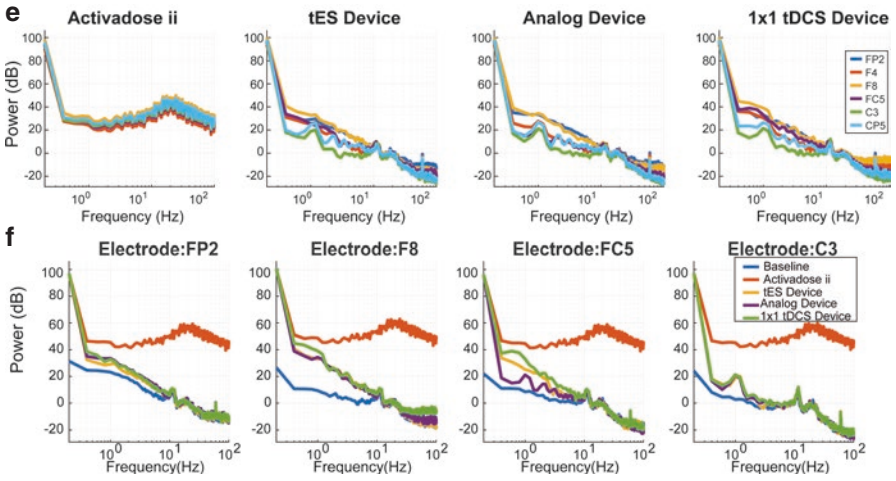

Fig. 11.5 (continued)

The DC offset can sometimes change incrementally ("drift") while stimulation is sustained (Hahn et al. 2013), this fractional change (up to ~ 3 mV or 2% of the DC offset over 50 secs with 2 mA of current) is still larger than EEG signals in general. Residual DC offset post stimulation can also be evident for up to approximately 1 min after the end of the ramp down (Fig. 11.2c). These residual voltages are significantly less than the peak DC offset during stimulation (~1.5 mV) but are on the order of magnitude of drift in the DC offset during stimulation. The spatial distribution of the scalp topography of the residual DC offset (scalp voltage after stimulation) is comparable to that of the DC offset during stimulation (scalp voltage during stimulation), where it has the largest positive and negative values near the anode and cathode electrodes, respectively (See Fig. 11.5b Post Stim).

Characteristics of the Spectral Profile

By utilizing spectrograms, the broadband harmonic distortions created during the ramp-up/ramp-down periods of the stimulators as a result of the stepwise escalation/de-escalation of current and resultant stepwise voltage offset can be easily illustrated (Fig. 11.5d). The distortions created during the ramp-up/ramp-down periods introduce broadband noise that contaminate these period of online stimulation EEG data and can be difficult to attenuate during post processing. After ramp-up though, this broadband step-wise contamination is eliminated during the delivery of the DC. During stimulation, significant power at low frequency (~0 Hz) reflect the DC offset. Overall low frequency activity (<10 Hz), also has increased power compared to no stimulation conditions. The reduced but significant DC offset post stimulation is also apparent and should be noted (See period after ramp-down in Fig. 11.5d).

With online stimulation, EEG features like inherent alpha activity (8–12 Hz) can be resolved with proper frequency windowing. In some cases, spectrograms can reveal increased low frequency activity (1–1.2 Hz) during but not pre or post stimulation, with higher power near stimulation electrodes (see also Fig. 11.5e). For example, clear 1–1.2 Hz peaks are observed at electrode C3, nearest the cathode (C5), whereas at electrodes FP2 and F8 such prominent peaks are not evident (possibly due to blink interference at frontal channels; Fig. 11.5f).

Linearity of DC Voltage

With Bifrontal stimulation (anode:AF7, cathode: AF8), EEG electrodes closest to the anode exhibit a positive voltage offset and those near the cathode exhibit a negative voltage offset; whereas the opposite polarities can be seen at the aforementioned electrodes when the stimulation polarities are switched (anode:AF8, cathode:AF7; Fig. 11.6a). In this case electrodes F7 and F8 exhibited the highest voltage changes, whereas those further away from the stimulating electrodes exhibited a smaller change in voltage during stimulation (Fig. 11.6b).

When the current intensity is increased (from 0.5 to 2.0 mA), scalp topographies show increases in the area of the high voltage offsets (both negative and positive depending on the montage used; Fig. 11.6b). When applying a series of different current intensities (i.e. 0.5, 1.0 1.5, 2.0 mA) over the course of one EEG recording, the mean voltage offset for repeated current intensities are linearly correlated across the majority of EEG electrodes (Fig. 11.6c). This is true for different current polarities as well (i.e. switching the anode and cathode). In other words, the voltage offset changes linearly between applied current intensities. Although electrodes further away from the stimulation sites do not exhibit large voltage offsets, they do show a linear relationship across applied stimulation intensities. Taking the topographic difference between stimulation intensities results in a slope computation across the scalp and shows that the change in voltage between current intensities has identical spatial patterning across the scalp (Fig. 11.6d). This demonstrates that although there is a large voltage change between stimulation intensities the slope or increase in voltage (mV/mA) remains similar between stimulation intensities.

Inherent Physiologic Artifacts

Inherent physiological artifacts can be characterized as artifacts that are independent of stimulators as well as EEG devices and that result from physiologic integration with the overall DC artifact produced by stimulation (see Fig. 11.5a). These physiologic artifacts that occur during stimulation can range over a broad spectrum of physiologic processes, however here we highlight four types of physiological distortions that are seen during concurrent EEG and tDCS. These include cardiac

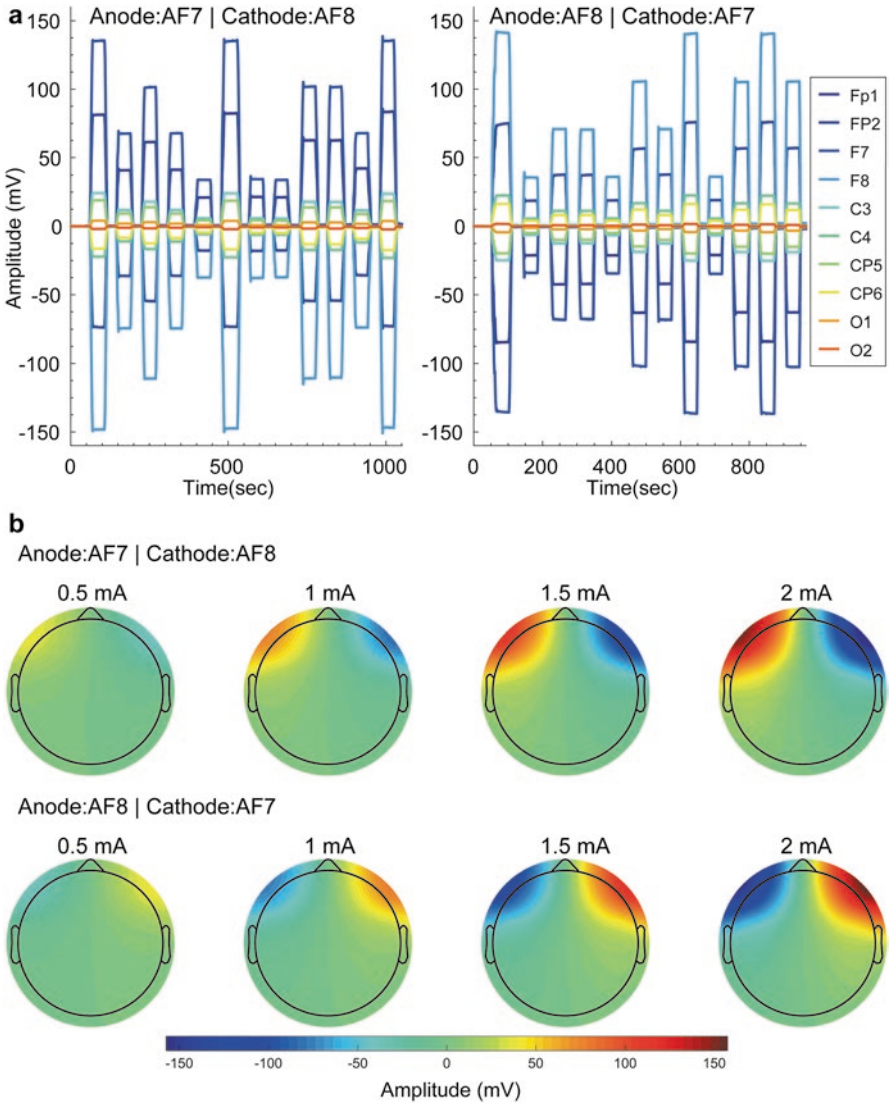

Fig. 11.6 (**a**) EEG voltage over time with online stimulation and EEG. The DC voltage offset can be seen when randomized current intensities between 0.5–2.0 mA are applied and removed over time. The largest DC voltage offset is seen at electrodes closest to the anode and cathode. (**b**) For Bifrontal stimulation frontal EEG electrodes have the largest increase (negatively and positively) with increasing current intensity. Areas under the anode have large positive offsets whereas those under the cathode have larger negative offsets. (**c**) The mean voltage offset across applied current intensities for both stimulation polarities are linearly correlated across the majority of EEG electrodes. (**d**) The change in voltage between current intensities (mV/mA) have identical spatial patterning across the scalp for different current intensities. This spatial patterning is consistent across current intensities applied for both stimulation polarities

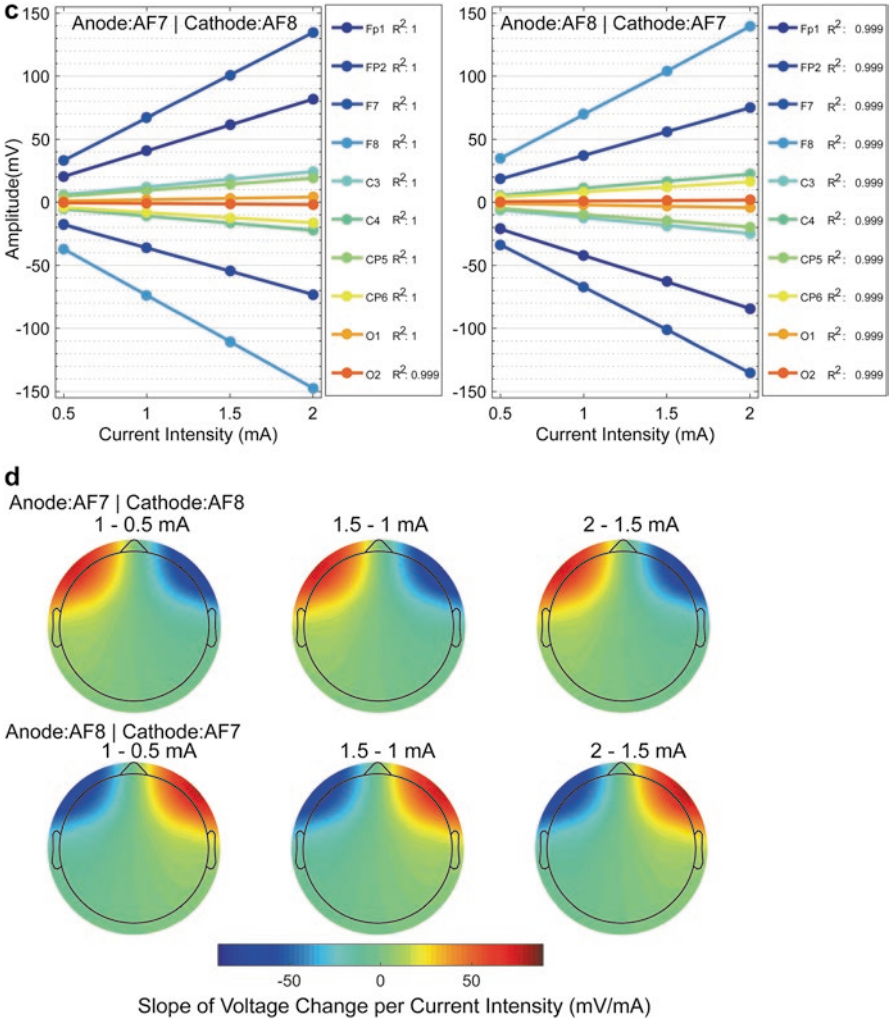

Fig. 11.6 (continued)

artifacts, oculomotor artifacts, myogenic artifacts, and DC drift artifacts. We also talk about the use of computational head models, which can be used to model and understand the dynamics and sources of these artifacts.

We define "physiologic stimulation artifacts" as real changes in the voltage on scalp that reflect physical interaction of applied current with the body – by definition these artifacts are then inherent (or unavoidable) to any stimulation or recording hardware. Of particular concern is if such physiologic artifacts, by failing to meet the assumptions above, may not be removed or properly attenuated by conventional signal processing techniques, leading to spurious conclusions. Identifying the mechanisms and features of physiologic artifacts allows for identifying and applying suitable signal processing and having greater confidence in outcomes.

Physiological Artifact: Cardiac Artifact

The cardiac artifact, sometimes referred to as a ballistocardiographic artifact or ballistocardiogram (Rubin and Daube 2016; Schmitt 2017), can be observed consistently during stimulation and is highly disruptive to acquired data. The artifact, which can sometimes resemble and be mistaken for stimulator shifts in voltage (Roy et al. 2014), is stimulation device independent (Fig. 11.7a, b), montage specific (see Fig. 11.7b, f), narrowband (Fig. 11.7c), and stimulation intensity specific (Fig. 11.7e).

When paired with concurrent electrocardiogram (ECG) the oscillatory cardiac artifact shows consistent peaks following the QRS complex but preceding the T-wave of the ECG (Fig. 11.7a). These cardiac related peaks can be observed across different types of DC stimulators, excluding iontophoresis devices which can introduce device related artifacts obscuring the cardiac artifact. The artifacts' peaks are also polarity dependent and montage specific indicating that it is strongest near stimulation electrodes (Fig. 11.7b). In the frequency domain, the cardiac artifact's activity is seen as a low frequency, heartbeat-locked peak at approximately 1 Hz (depending on subjects' heart rate; Fig. 11.7c). This activity is seen during but not before or after stimulation. Analogous to the DC offsets, this activity is present in electrodes closest to the stimulating electrodes in a montage specific manner. Since the cardiac artifact exhibits a slow rise and fall that is time locked relative to the R-wave of ECG signals and is montage specific; it is believed to be a mechanical cardiac signal amplified with local changes in skin impedance during stimulation (Noury et al. 2016).

The artifact can also be easily produced with currents as low as 0.5 mA and increases as more current is introduced during stimulation (Fig. 11.7e–g). The montage specificity is seen with the spatial scalp distribution of the cardiac artifact; a maximal negative deflection is present nearest the cathode and maximal positive deflection is present nearest the anode (Fig. 11.7b, f). EEG electrodes further away from the stimulating electrodes however do not exhibit significant voltage modulations resulting from the cardiac artifact.

Assuming a skin impedance change of 0.01% during stimulation, a computational model can be generated to simulate the cardiac artifact's spatial distribution and the magnitude of its voltage deflection. Incorporating the aforementioned assumptions, the computational models predict that for HD-Bifrontal stimulation, anterior recording electrodes would undergo higher voltage amplitude changes during a cardiac pulse, with decreasing voltage deviation with increasingly posterior electrode locations (Fig. 11.7g). These predictions corroborate the notion that tDCS first creates a montage specific distribution of scalp voltages that is then modulated at each pulse by a global change in scalp impedance.

The concerning aspects of the appearance of the cardiac artifact is its stimulation dependent amplitude as well as its time variant scalp distribution. With skin impedance being a dynamic factor, the cardiac artifact could be highly influenced by subjects' physiological and psychological state (Luft and Bhattacharya 2015) during stimulation where anxieties or fears during tDCS can cause a raise in heartbeat and increase sweating, nonlinearly altering acquired data. In electrodes adjacent to stimulation sites, the cardiac artifact can be seen to increase up to approximately

40 μV with 2 mA of current, which is larger than most event-related potentials (ERPs) (Dinteren et al. 2014) and raises concerns with previous concurrent online EEG and stimulation studies that have examined ERPs (Cunillera et al. 2015; Faehling and Plewnia 2016). Detectable changes in the overall voltage offset of the

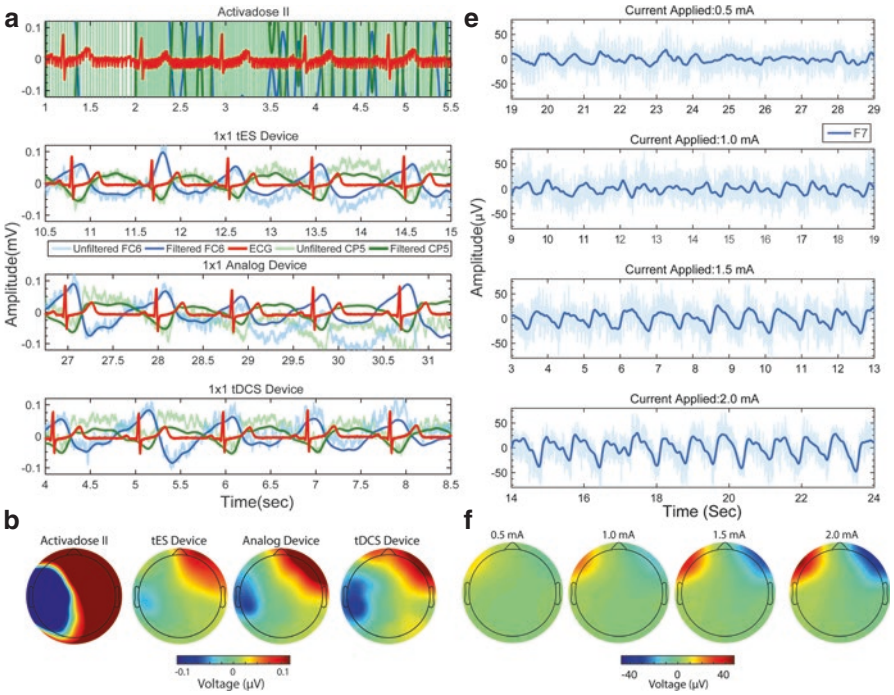

Fig. 11.7 (**a**) The cardiac artifact is reproducible with a range of stimulation devices, with the exception of the Activadose II, which produces large-amplitude, high-frequency broadband noise during stimulation in EEG data as well as in ECG electrodes. The cardiac artifact appears as consistent peaks following the QRS complex but preceding the T-wave of the ECG. Detrended traces for electrodes FC6 and CP5 are also present for comparison. (**b**) Scalp topographies during the peak of the cardiac artifact across stimulation devices show that the artifact is montage specific since the artifacts' spatial distribution is reflective of the stimulation montage. (**c**) A comparison of ECG; and EEG baseline (not powered), during, and post stimulation. A prominent peak at 1–1.2 Hz is present for both the ECG and EEG during stimulation conditions, but not for EEG baseline (not powered) and post stimulation. (**d**) ECG, ECG envelope, and respiration signal over time. During stimulation, the overall ECG signal has a pronounced DC offset. Linear changes in the ECG voltage during the stimulation ramp-up and ramp-down periods are also present. (**e**) The cardiac artifact over time with applied current intensities of 0.5, 1.0, 1.5, and 2.0 mA. (**f**) Mean scalp topographies at the peak of the cardiac artifact during 0.5, 1.0, 1.5, and 2.0 mA of applied current. (**g**) Mean and SEM of cardiac artifact peaks at electrodes F7 and F8 during stimulation for current intensities of 0.5, 1.0, 1.5, and 2.0 mA. (**h**) Computational model prediction of the spatial scalp distribution of the cardiac artifact during HD-Bifrontal stimulation

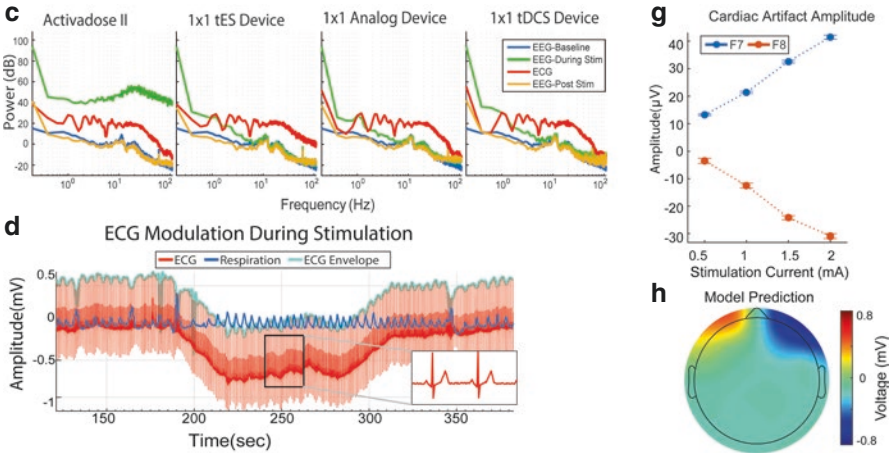

Fig. 11.7 (continued)

ECG signals (~0.5 mV), measured across the chest during stimulation, also raise further questions about how stimulation interacts with autonomic nervous system (Clancy et al. 2014; Schestatsky et al. 2013; Schroeder et al. 2015; Vandermeeren et al. 2010), which could in turn result in changes to the cardiac artifact, as well as heart rate or heart rate variability. In the clinical domain, studies examining the online effects of tDCS are cautioned when it comes to patients who have disorders affecting cardiac function. With the aforementioned studies, concurrent ECG with EEG monitoring is highly recommended. As such, patients with cardiac dysfunctions may introduce further variability to the already time variable cardiac artifacts, which can be misinterpreted as alterations in low frequency Delta activity in acquired EEG data. Reassuringly though, the artifact disappears with the removal of the DC current after both long and short periods of stimulation, attesting to the artifact's dynamics.

Physiological Artifact: Ocular Motor Artifact

During stimulation, strong modulatory effects are observed in relation to ocular motor or blink responses. Amplitudes of these physiologic responses can become highly variable across stimulation current intensities as well as across stimulation montages. The spatial distribution during blink responses become altered during stimulation, in a stimulation montage specific manner.

Depending on the montage used and compared to baseline or no stimulation conditions, the blink artifact amplitude increases, inverts in polarity, or becomes unrecognizably low in amplitude that it appears to be suppressed (see Fig. 11.8a).

These alterations are consistent across DC stimulators (Fig. 11.8b). Interestingly, the latency of the blink propagation between the left and right eye remains unaltered; remaining time-locked under pre, during, and post stimulation conditions. Near the anode, where a positive scalp voltage is present, blink artifacts have large decreases in amplitude opposed to near the cathode, where a negative scalp voltage

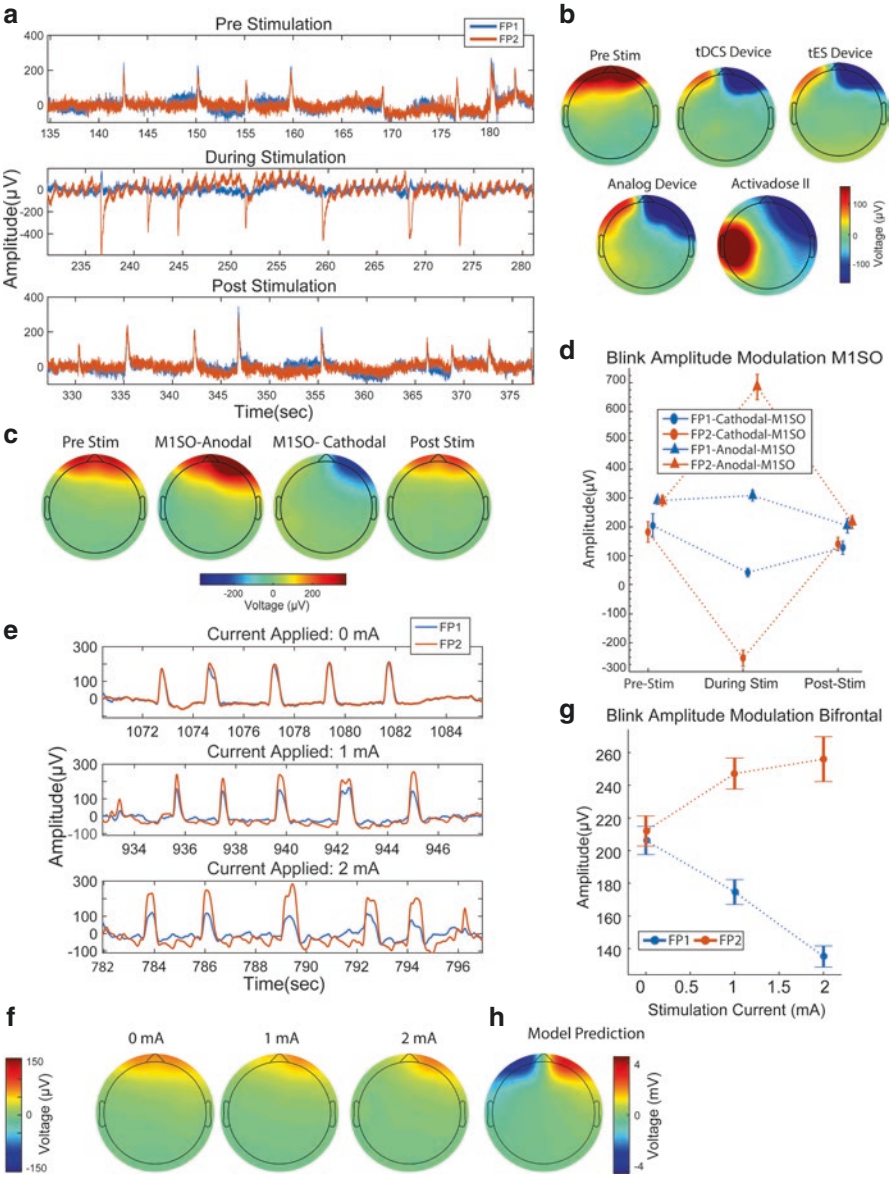

is present, where blink artifacts have large increases in voltage during stimulation (Fig. 11.8c, d). Within stimulation montages the ocular motor amplitude modulation linearly increases or decreases with stimulation intensity (Fig. 11.8e–g). These dramatic changes in amplitude are believed to be a result of eyelid closure with possible smaller contributions from the shifting of the eyes' retinocorneal dipole (Berg and Scherg 1991; Iwasaki et al. 2005). With the eyelids closing during stimulation, they considerably alter the path of the applied current on the scalp and distort the resultant positive amplitude normally seen with Cz referential montages.

These alterations pose problems for automatic artifact rejection algorithms since during stimulation the blink artifact becomes highly distorted in some cases. Previous studies examining tDCS effects on blink responses in healthy subjects using electrooculogram (EOG; Beyer et al. 2017; Cabib et al. 2016; Zuchowski et al. 2014) may also be affected by these artifactual voltage modulations. Similarly, any future studies in the clinical domain using EOG as an online biomarker in tDCS trials with disorders including Parkinson's disease, or multiple sclerosis, would be cautioned. As with other physiologic artifacts the use of traditional control experiments (changing montage) and some signal processing corrections may not suffice. Fortunately though the topographic spatial distribution of scalp voltages during blinks were somewhat predictable based on the overall average topographic scalp distribution during stimulation, which could provide means for development of more dynamic blink artifact rejection methods.

To model the nature of the altered blink responses during concurrent EEG and stimulation computational models can be utilized. In order to model simplistic blink responses, skin over the eye (eyelids) are removed from the computational head

Fig. 11.8 (**a**) During the pre and post-stimulation time periods, both FP1 and FP2 detect positive blink deflections. During the course of cathodal M1SO (referring to cathode:C3, anode:AF8) stimulation the blink responses at FP2 (near the anode) reverse in polarity and show a high amplitude negative deflection, whereas blink responses at FP1 decrease in amplitude and maintain a diminished but positive polarity. (**b**) A comparison of blink responses across stimulating devices compared to pre-stimulation. During stimulation a negative monopole is present in electrodes over the right SO locations (near the anode) and a positive monopole is present in electrodes over the left SO locations, across devices (with the exception of the Activadose II) for the application of 2 mA of cathodal M1SO stimulation, whereas Bifrontal positive dipoles are present over both eyes, pre- stimulation. (**c**) Blink scalp topographies for pre-stimulation, during 1 mA of anodal M1SO stimulation (cathode:AF8, anode:C3), during 1 mA of cathodal M1SO stimulation (cathode:C3, anode:AF8), and post-stimulation conditions. (**d**) Mean and SEM of blink amplitudes at electrodes FP1 and FP2 during 1 mA of M1SO anodal and cathodal stimulation, compared to pre and post-stimulation blink responses. (**e**) Blink responses at FP1 and FP2 over time during 0, 1, and 2 mA of current with a Bifrontal stimulation montage. As the current intensity increases the difference between peak blink amplitude, between FP1 and FP2, increases. (**f**) Blink scalp topographies during 0, 1, and 2 mA of current with a Bifrontal stimulation montage. (**g**) Mean and SEM of blink amplitudes at electrodes FP1 and FP2 for 0 mA, 1 mA, and 2 mA of applied current with a Bifrontal stimulation montage. As the current intensity increases the difference in peak amplitudes between FP1 and FP2 becomes larger. (**h**) Computational model prediction of blink scalp topography during HD-Bifrontal stimulation

models. The difference between model predictions during stimulation with and without eyelids produced an overall scalp topography akin to that seen during EEG. Like topographic voltage distribution seen during EEG, the model prediction demonstrates that with Bifrontal stimulation there is an elevated left SO positive voltage and an elevated right SO negative voltage (Fig. 11.8h). These predictions support the notion that blink responses increase near the cathode whereas they decreased near the anode.

Physiological Artifact: Myogenic Distortions

During stimulation myogenic artifacts, related to facial muscle contraction or jaw clenches, are seen to be montage specific, broadband, and are highly modulated in a current intensity specific manner (Fig. 11.9a–c), similar to the blink and cardiac artifacts. With higher current intensities, the overall broadband activity shifts in amplitude depending on the stimulation montage used. Increasing current intensity, introduces a low frequency drift to the high frequency muscle activity, during muscle contraction. This activity is variable across the scalp and the divergence in amplitude between left and right hemispheric high frequency activity increases with increased bilaterally applied current (HD-Bifrontal; Fig. 11.9a, b). In terms of spatial scalp location, during stimulation and jaw clenching, the DC alters the distribution and polarity of the muscle activity seen on the scalp, compared to muscle activity without stimulation (Fig. 11.9c).

Myogenic interactions during EEG, specifically electromyography (EMG) without stimulation, are the result of contractions of primarily the masseter, temporalis and frontalis muscles (Goncharova et al. 2003; Whitham et al. 2007). These contractions can significantly contaminate acquired data due to its high amplitude, and broadband spectral and anatomical overlap with neurogenic sources (Barlow 1985; Shackman et al. 2009). When combined with stimulation, these myogenic distortions become exacerbated and with their overlap with neurogenic sources, makes it even more difficult for correction algorithms to separate both sources. These myogenic interactions, like the cardiac artifact, can be influenced by subjects' physiological and psychological state (Bradley et al. 2001; Coan and Allen 2003; Tassinary et al. 2007; Waterink and van Boxtel 1994), resulting in variable muscle activation. Even weak facial muscle contractions have been shown to produce low frequency EEG activity that can be mistaken for changes in cognitive related frequency bands like Alpha rhythms (Goncharova et al. 2003; Lee and Buchsbaum 1987; Willis et al. 1993), which can be especially concerning when these artifacts are accentuated by stimulation currents. In the clinical setting, these EMG artifacts may appear in patients with conditions including facial myokymia, hemifacial spasm, or palatal myoclonus (Westmoreland 1996). Caution should be taken in cases like these and other disorders affecting myogenic activity since coupled with stimulation, resultant

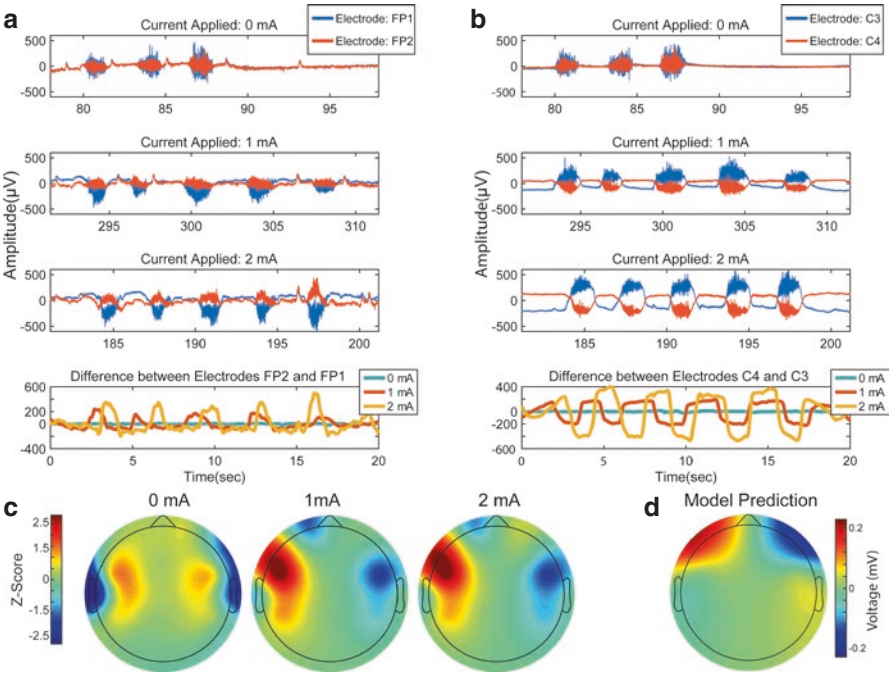

Fig. 11.9 (**a**) Jaw clenches over time detected at bilateral electrodes FP1 and FP2 for applied currents of 0, 1, and 2 mA. Currents were applied in a HD-Bifrontal montage and voltages at FP1 (near the anode) diverged negatively from FP2 with increasing current. (**b**) Jaw clenches over time at bilateral electrodes C3 and C4 for applied currents of 0, 1, and 2 mA. Currents were applied in a HD-Bifrontal montage and voltages at C3 (near the anode) diverged positively from C4 with increasing current. (**c**) Average scalp topographies during jaw clenches plotted as z-scores for comparison. (**d**) Computational model prediction of the spatial scalp distribution of EMG activity resulting from jaw clenches during stimulation

artifacts can be misinterpreted as epileptiform activity or modulations in the frequency domain. These modulations with stimulation however, did not outlast the duration of stimulation and disappeared as the external current was removed.

In order to model EMG activity resulting from jaw clenches during stimulation, the masseter and temporalis muscles are incorporated into MRI-derived computational models. Muscle fibers are represented over the mandible for the masseter muscle and over temporal regions of the skull for the temporalis muscles. The scalp voltages produced by tDCS are then computed with either "relaxed" muscle properties assigned or "active" muscle properties – assuming a 1% muscle conductivity change during to muscle fiber activation. The difference in scalp voltages between the two models gives a prediction of the spatial profile of the myogenic artifact. This muscle activity on the scalp during stimulation, are in accord with the overall DC

produced with EEG derived voltages, but do not fully capture the voltage shift during muscle contraction (Fig. 11.9d).

Physiological Artifact: DC Drift

The physiologically related DC drift artifact usually arises from increased perspiration on the scalp (Klass 1995), which consequently alters skin impedance. During EEG this physiologically related DC drift usually takes the form of a low frequency (<0.5 Hz), high amplitude wave (Corby et al. 1974; Picton and Hillyard 1972). During concurrent tDCS and EEG, this non-stationary physiologic artifact can be exacerbated with the introduction of a DC current. With stimulation, this artifact can be high amplitude, low-frequency, narrowbanded, change over the course of the stimulation session, montage specific (normally localized nearest the points of high perspiration, however strongest effect can be seen nearest stimulating electrodes during tDCS), and under some circumstances outlast the duration of stimulation if left unattended. Although not detrimental to data quality since the artifact can be attenuated in post processing, care should be taken to avoid such artifacts in order to acquire the highest quality of EEG data.

Inherent Stimulator Artifacts

With concurrent HD-tDCS and EEG, one source of significant extraphysiologic noise introduction can arise from the stimulators themselves. Stimulators that produce variable current outputs and not a constant direct current can distort and decimate the voltage profile of acquired EEG. These artifacts, referred to as inherent stimulator artifacts, are described as artifacts that are universal to any stimulator/EEG system used, however its severity or impact on data quality is variable. Inherent stimulator artifacts can be divided into three main types of artifactual distortions: broadband noise artifact, "on noise" artifact, and DC-offset artifact.

The broadband noise artifact describes the fact that, under ideal conditions, no simulator can generate an ideal DC without the introduction of power at unintended frequencies. This type of artifact, as its name suggests, produces distortion or nonlinear modulations of both signal and noise across several frequencies (hence broadband) including those of physiologic interest with EEG. With this type of artifact, during tDCS the highest modulation can be seen around 0 Hz (the DC frequency) when compared to pre stimulation or no stimulation conditions (device off baseline). The broadband noise artifact can also change over the course of a stimulation session as a result of stimulator reactivity or impedance changes on the scalp. This

type of artifact usually does not outlast stimulation and usually disappears after the stimulator is turned off, however residual scalp voltages together with skin impedance changes post stimulation can produce low frequency broadband modulations (see Fig. 11.7c). When it comes to the artifacts spatial variation on the scalp, the broadband noise artifact is seen to be montage and current intensity specific, having maximal distortion in EEG electrodes nearest to the stimulating electrodes in a manner reflective of/tracing the scalp DC voltage.

The "On noise" artifact is the result of leakage or injection of stimulator noise into the recording electrodes while the stimulating device is on yet not stimulating (See time zero onwards in Fig. 11.10a). In some cases large voltage offsets can be seen when the stimulation device is turned on and noise can occur when these devices check impedances before stimulation. This type of artifact has been shown to be broadband, montage specific, additive, and can possibly outlast stimulation if the stimulation device is left connected and on.

The DC-Offset artifact refers to the large voltage offset produced during stimulation (See during stimulation period Fig. 11.2a). This offset, under ideal stimulator and EEG data acquisition conditions, is stable and linear; however, the DC-offset can be somewhat non-stationary and fluctuate over the course of stimulation due to physiologic changes in scalp impedance or subject perspiration. Under non-ideal hardware conditions slow dynamic changes can be seen as the result of the stimulator used, in that the stimulator does not produce a stable DC current; as a result of impedance changes within the stimulator; or as a result of non-linear EEG amplifier performance if voltages reach amplifier limitations.

Non-inherent Artifacts

Artifacts created as a result of non-ideal experimental conditions or set-up can be classified as non-inherent artifacts. These artifacts can easily arise if quality control is not met or strict data monitoring is not performed. Although non-inherent artifacts span a wide range of classifications, here we focus on stimulation and movement distortion, EEG saturation, EEG distortion, and electrode bridging.

Similar to myogenic artifacts, movement disruption during EEG and stimulation can result in robust signal distortion of neural signal. Abrupt or slow head rotation or tilting can introduce broadband noise and in some cases fully distort neural activity during concurrent stimulation and EEG. When examined with concurrent displacement recordings in the X, Y and Z, directions from Cz; spectrograms over time and frequency show that during 2 mA M1SO (anode M1) stimulation, slow neck rolling motions greatly disrupted acquired data. EEG electrodes nearest to the stimulating electrodes (F8) show the largest distortions over time and frequency whereas those further away show lesser distortions (O2; Fig. 11.10b, c). Correlations of EEG

electrodes and accelerometer deflections corroborate the notion that the distortions seen in EEG channels during head motion are related to the movement of the head and electrodes, which is most likely exacerbated or amplified by the applied DC. These distortions in most cases are the result of slight movement of the stimulating electrodes as well as the recording EEG electrodes on the scalp. Together with stimulation these distortions are stimulation montage and current intensity dependent, can change over the course of stimulation, and do not outlast the duration of stimulation (depending on the subject). To avoid this, subjects should be comfortably seated and instructed to minimize movement during stimulation and data acquisition. In some cases a headrest can be utilized to keep subjects head in place during experimental procedures.

EEG saturation can occur regardless of stimulation introduction. Saturation occurs when the dynamic range of EEG amplifiers have been reached and EEG signals become "clipped" or do not register voltages above or below a certain range (Light et al. 2010). Amplifier gain settings can, in some cases, influence the dynamic range of the data being acquired and bring the data closer to saturation if gain settings are too high. With concurrent stimulation and EEG this issue can arise very easily and frequently. Since tDCS creates/injects a large voltage offset in EEG recording electrodes, these electrodes become shifted towards their saturation point, designated by the dynamic range of the EEG amplifiers. For example, in Fig. 11.10d current was gradually ramped up during concurrent EEG where the amplifier gain was increased (prior to the commencement of stimulation). Electrodes closest to the anode and cathode (F7 and P8) saturated much sooner than those further away (FP1 and O2), as indicated by the derivative of the EEG voltage (lighter colors) over time (Fig. 11.10d). As the saturation point was reached, the derivative of the EEG voltage over time became zero and voltages beyond the dynamic range of the amplifier were no longer recordable. When the EEG electrodes saturate the data recorded cannot be utilized since any underlying neural data is obliterated. This type of stimulation-related saturated data is usually not broadband, can change during a stimulation session, is highly montage specific, and can sometimes outlast stimulation.

When EEG signals approach the ends of the dynamic range of amplifiers, they can sometimes enter a non-linear amplification range in the EEG amplifiers used. Within this non-linear region EEG signals can sometimes become highly distorted and artifactual. This type of artifact is usually broadband, can change during a stimulation session, is montage specific, and disappears after stimulation ends if it is strictly stimulation related. This type of saturation can be avoided by ensuring that EEG amplifiers that are used have an adequate dynamic range to accommodate large voltage fluctuations.

Electrode bridging in EEG often occurs when too much electrolyte gel is introduced between the scalp electrode interface and the gel merges with neighboring

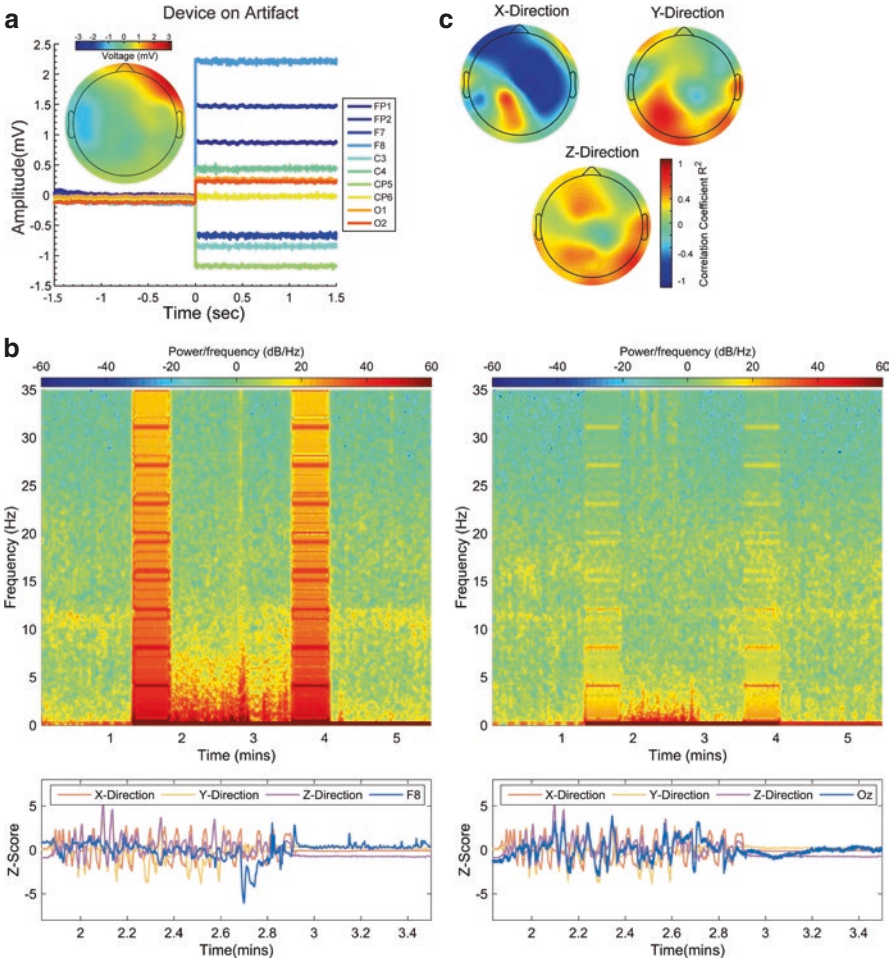

Fig. 11.10 (**a**) Device "On Noise" where time zero onwards indicates the time the stimulation device was switched on but not stimulating. Scalp topography displays the difference in voltage between device on and device off, after zero and before zero respectively. (**b**) Spectrograms at electrodes F8 and O2 over the course of pre, during, and post stimulation with the subject making several head movements during stimulation. EEG electrodes are presented with concurrent time-locked accelerometer recordings, each indicating the direction of displacement. (**c**) Correlation of accelerometer displacement with EEG voltage distortion over time, over the course of stimulation and head movement. (**d**) Electrode saturation over time with increasing current intensity. As current is increased electrodes (F7 and P8) closest to stimulating electrodes saturated earlier in time than those further away (FP1 and O2). Darker colors indicate electrode voltage over time whereas lighter colors indicate the derivative of the voltage over time. When the derivative becomes zero, saturation is reached

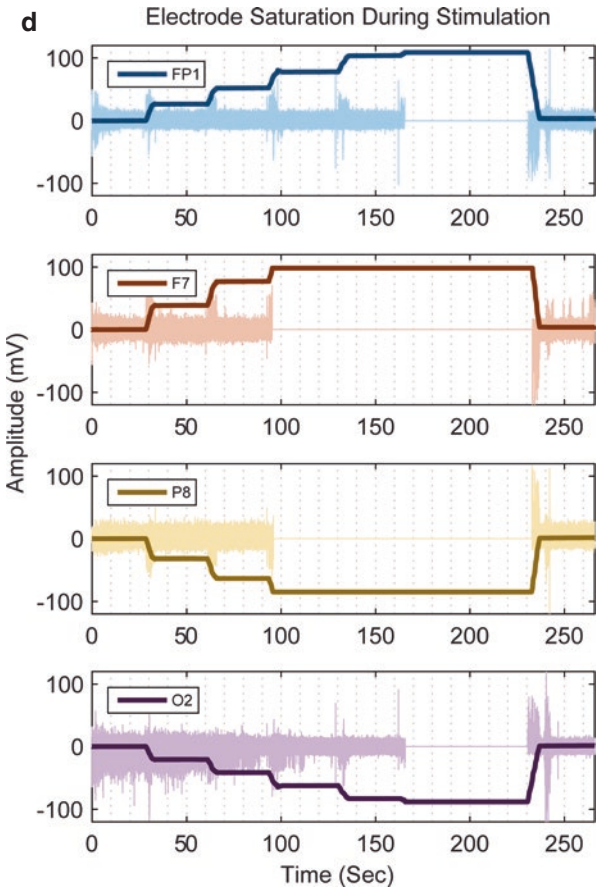

Fig. 11.10 (continued)

recording sites creating low impedance electrical bridges between two or more neighboring electrodes (Alschuler et al. 2014; Greischar et al. 2004; Tenke and Kayser 2001). This issue could be further exacerbated with environmental factors like room temperature that can result in increased scalp perspiration in subjects, which can also act as an electrolyte bridge. In terms of data quality, electrode bridging results in false identical signals being received by multiple electrodes that are bridged. In terms of tDCS though, the effects of electrode bridging of either stimulation electrodes, recording electrodes, or a combination of both; on acquired data can be detrimental. Electrode bridges during stimulation and EEG can result in robust current shunting across the scalp. Not only does the current not reach its

proper target but it also gets introduced directly into the EEG recording electrodes distorting any neural data being recorded. Bridging can be avoided by utilizing an appropriate amount of electrolyte gel or saline at recording sites and at stimulation sites. Also ensuring that EEG caps adequately fit (not too tight or too loose), are not moved or do not shift over the course of procedures can help in avoiding bridging.

Artifact Removal

In order to realize the promise of combined EEG-tDCS, it is necessary to develop robust techniques for removing or otherwise mitigating the aforementioned artifacts. Although no straightforward approach exists, due to the robustness of said artifacts, some signal processing techniques exist for cleaning up some aspects of acquired concurrent online EEG- stimulation data. One common feature of all these artifacts is that they possess a seemingly stable spatial topography that is closely related to the tDCS montage. As a result, spatial filtering based techniques that estimate the (spatial) subspace of the artifact may be able to remove a significant proportion of the artifact variance. By regressing the corrupted EEG onto the artifact's subspace and then subtracting the projections (Parra et al. 2005), a large part of the artifact variance should vanish. Unfortunately, even a small amount of residual variability will likely have a confounding effect on any subsequent analysis, as the raw power of the artifacts is very large. It is worth pointing out that this problem is analogous to the one faced when recording EEG in the fMRI environment where artifacts are similarly large (Allen et al. 2000; Niazy et al. 2005). Previous works have employed multistage techniques for removing the residual artifact from the EEG recorded during tACS (Helfrich et al. 2014) and some of these can be adapted for tDCS.

Summary

Integration of tDCS with MRI/MRS, NIRS, and EEG holds great promise for shedding light on the underlying neural mechanisms of stimulation effects. While integration with these methods requires special consideration, a growing body of work provides both evidence of feasibility as well as insight into solutions to common concerns. Integration may not be easily achieved in certain cases, but clearly understand the current limitations of integration is an important first step in designing effective and interpretable studies. In addition, this information provides a clear guide to areas of tDCS integration that require future study and

refinement. Regardless of current limitations, recent work in the integration of tDCS with modern neuroscience methods has produced critical insight into tDCS neural mechanisms and provides clear evidence of feasibility. Integration of these methods provide a platform for understanding brain behavior relationships using the inherent strengths of each approaches: tDCS providing a method for directly intervening on brain tissue, EEG providing high degrees of temporal resolution in brain processing, MRI providing a high degree of spatial resolution for structural and functional brain function, MRS providing insight into neurometabolite and neurotransmitter concentrations in brain tissue, and NIRS providing both spatial and temporal resolution of brain activity near the surface of the cortex. This methodological toolbox can be used to answer a wide range of questions about the brain and behavior, as well as underlying neural mechanisms of treatment response and efficacy. In addition, the potential for using this information to better optimize tDCS treatment studies is an exciting frontier in the field. As this field of study grows and our methodological understanding of integration process improves, the range of testable hypotheses about tDCS and the brain will only expand.

References

Aasted, C. M., Yücel, M. A., Cooper, R. J., Dubb, J., Tsuzuki, D., Becerra, L., … Boas, D. A. (2015). Anatomical guidance for functional near-infrared spectroscopy: AtlasViewer tutorial. *Neurophotonics, 2*, 20801.

Abbott, N. J., Rönnbäck, L., & Hansson, E. (2006). Astrocyte–endothelial interactions at the blood–brain barrier. *Nature Reviews. Neuroscience, 7*, 41–53.

Al-Kaysi, A. M., Al-Ani, A., Loo, C. K., Powell, T. Y., Martin, D. M., Breakspear, M., & Boonstra, T. W. (2016). Predicting tDCS treatment outcomes of patients with major depressive disorder using automated EEG classification. *Journal of Affective Disorders, 208*, 597–603.

Allen, P. J., Josephs, O., & Turner, R. (2000). A method for removing imaging artifact from continuous EEG recorded during functional MRI. *NeuroImage, 12*, 230–239.

Alschuler, D. M., Tenke, C. E., Bruder, G. E., & Kayser, J. (2014). Identifying electrode bridging from electrical distance distributions: A survey of publicly-available EEG data using a new method. *Clinical Neurophysiology, 125*, 484–490.

Amadi, U., Ilie, A., Johansen-Berg, H., & Stagg, C. J. (2014). Polarity-specific effects of motor transcranial direct current stimulation on fMRI resting state networks. *NeuroImage, 88*, 155–161.

Antal, A., Bikson, M., Datta, A., Lafon, B., Dechent, P., Parra, L. C., & Paulus, W. (2014). Imaging artifacts induced by electrical stimulation during conventional fMRI of the brain. *NeuroImage, 85*(Pt 3), 1040–1047.

Antal, A., Polania, R., Schmidt-Samoa, C., Dechent, P., & Paulus, W. (2011). Transcranial direct current stimulation over the primary motor cortex during fMRI. *NeuroImage, 55*, 590–596.

Aroniadou, V. A., & Keller, A. (1995). Mechanisms of LTP induction in rat motor cortex in vitro. *Cerebral Cortex, 5*, 353–362.

Attwell, D., Buchan, A. M., Charpak, S., Lauritzen, M., MacVicar, B. A., & Newman, E. A. (2010). Glial and neuronal control of brain blood flow. *Nature, 468*, 232–243.

Bachtiar, V., Near, J., Johansen-Berg, H., & Stagg, C. J. (2015). Modulation of GABA and resting state functional connectivity by transcranial direct current stimulation. *eLife, 4*, e08789.

Barlow, J. S. (1985). A general-purpose automatic multichannel electronic switch for EEG artifact elimination. *Electroencephalography and Clinical Neurophysiology, 60*, 174–176.

Baudewig, J., Nitsche, M. A., Paulus, W., & Frahm, J. (2001a). Regional modulation of BOLD MRI responses to human sensorimotor activation by transcranial direct current stimulation. *Magnetic Resonance in Medicine, 45*, 196–201.

Baudewig, J., Siebner, H. R., Bestmann, S., Tergau, F., Tings, T., Paulus, W., & Frahm, J. (2001b). Functional MRI of cortical activations induced by transcranial magnetic stimulation (TMS). *Neuroreport, 12*, 3543–3548.

Bazargani, N., & Attwell, D. (2016). Astrocyte calcium signaling: The third wave. *Nature Neuroscience, 19*, 182–189.

Beckmann, C. F., Deluca, M., Devlin, J. T., & Smith, S. M. (2005). Investigations into resting-state connectivity using independent component analysis. *Philosophical Transactions of the Royal Society B: Biological Sciences, 360*, 1001–1013.

Berg, P., & Scherg, M. (1991). Dipole models of eye movements and blinks. *Electroencephalography and Clinical Neurophysiology, 79*, 36–44.

Beyer, L., Batsikadze, G., Timmann, D., & Gerwig, M. (2017). Cerebellar tDCS effects on conditioned Eyeblinks using different electrode placements and stimulation protocols. *Frontiers in Human Neuroscience, 11*, 23.

Binkofski, F., Loebig, M., Jauch-Chara, K., Bergmann, S., Melchert, U. H., Scholand-Engler, H. G., … Oltmanns, K. M. (2011). Brain energy consumption induced by electrical stimulation promotes systemic glucose uptake. *Biological Psychiatry, 70*, 690–695.

Boas, D. A., Culver, J., Stott, J., & Dunn, A. (2002). Three dimensional Monte Carlo code for photon migration through complex heterogeneous media including the adult human head. *Optics Express, 10*, 159–170.

Boggio, P. S., Ferrucci, R., Rigonatti, S. P., Covre, P., Nitsche, M., Pascual-Leone, A., & Fregni, F. (2006). Effects of transcranial direct current stimulation on working memory in patients with Parkinson's disease. *Journal of the Neurological Sciences, 249*, 31–38.

Bonnet, P., Rusch, N. J., & Harder, D. R. (1991). Characterization of an outward K+ current in freshly dispersed cerebral arterial muscle cells. *Pflügers Archiv European Journal of Physiology, 418*, 292–296.

Bottomley, P. A., Edelstein, W. A., Foster, T. H., & Adams, W. A. (1985). In vivo solvent-suppressed localized hydrogen nuclear magnetic resonance spectroscopy: A window to metabolism? *Proceedings of the National Academy of Sciences of the United States of America, 82*, 2148–2152.

Bozzo, L., Puyal, J., & Chatton, J.-Y. (2013). Lactate modulates the activity of primary cortical neurons through a receptor-mediated pathway. *PLoS One, 8*, e71721.

Bradley, M. M., Codispoti, M., Cuthbert, B. N., & Lang, P. J. (2001). Emotion and motivation I: Defensive and appetitive reactions in picture processing. *Emotion, 1*, 276–298.

Brayden, J. E. (1996). Potassium channels in vascular smooth muscle. *Clinical and Experimental Pharmacology & Physiology, 23*, 1069–1076.

Brunoni, A. R., Nitsche, M. A., Bolognini, N., Bikson, M., Wagner, T., Merabet, L., … Fregni, F. (2012). Clinical research with transcranial direct current stimulation (tDCS): Challenges and future directions. *Brain Stimulation, 5*, 175–195.

Buch, E. R., Santarnecchi, E., Antal, A., Born, J., Celnik, P. A., Classen, J., … Cohen, L. G. (2017). Effects of tDCS on motor learning and memory formation: A consensus and critical position paper. *Clinical Neurophysiology, 128*, 589–603.

Cabib, C., Cipullo, F., Morales, M., & Valls-Sole, J. (2016). Transcranial direct current stimulation (tDCS) enhances the excitability of Trigemino-facial reflex circuits. *Brain Stimulation, 9*, 218–224.

Cancelli, A., Cottone, C., Tecchio, F., Truong, D. Q., Dmochowski, J., & Bikson, M. (2016). A simple method for EEG guided transcranial electrical stimulation without models. *Journal of Neural Engineering, 13*, 36022.

Castro-Alamancos, M. A., Donoghue, J. P., & Connors, B. W. (1995). Different forms of synaptic plasticity in somatosensory and motor areas of the neocortex. *The Journal of Neuroscience, 15*, 5324–5333.

Charvet, L. E., Kasschau, M., Datta, A., Knotkova, H., Stevens, M. C., Alonzo, A., … Bikson, M. (2015). Remotely-supervised transcranial direct current stimulation (tDCS) for clinical trials: Guidelines for technology and protocols. *Frontiers in Systems Neuroscience, 9*, 26.

Chhabria, K., & Chakravarthy, V. S. (2016). Low-dimensional models of "neuro-Glio-vascular unit" for describing neural dynamics under normal and energy-starved conditions. *Stroke, 7*, 24.

Clancy, J. A., Johnson, R., Raw, R., Deuchars, S. A., & Deuchars, J. (2014). Anodal transcranial direct current stimulation (tDCS) over the motor cortex increases sympathetic nerve activity. *Brain Stimulation, 7*, 97–104.

Clark, V. P., Coffman, B. A., Trumbo, M. C., & Gasparovic, C. (2011). Transcranial direct current stimulation (tDCS) produces localized and specific alterations in neurochemistry: A ^{1}H magnetic resonance spectroscopy study. *Neuroscience Letters, 500*, 67–71.

Coan, J. A., & Allen, J. J. B. (2003). Varieties of emotional experience during voluntary emotional facial expressions. *Annals of the New York Academy of Sciences, 1000*, 375–379.

Cole, D. M., Smith, S. M., & Beckmann, C. F. (2010). Advances and pitfalls in the analysis and interpretation of resting-state FMRI data. *Frontiers in Systems Neuroscience, 4*, 8.

Corby, J. C., Roth, W. T., & Kopell, B. S. (1974). Prevalence and methods of control of the cephalic skin potential EEG artifact. *Psychophysiology, 11*, 350–360.

Cunillera, T., Brignani, D., Cucurell, D., Fuentemilla, L., & Miniussi, C. (2015). The right inferior frontal cortex in response inhibition: A tDCS-ERP co-registration study. *NeuroImage, 140*, 66–75.

Datta, A., Baker, J. M., Bikson, M., & Fridriksson, J. (2011). Individualized model predicts brain current flow during transcranial direct-current stimulation treatment in responsive stroke patient. *Brain Stimulation, 4*, 169–174.

Delpy, D. T., Arridge, S. R., Cope, M., Edwards, D., Reynolds, E. O. R., Richardson, C. E., … van der Zee, P. (1989). *Quantitation of pathlength in optical spectroscopy* (pp. 41–46). Boston, MA: Springer.

Dinteren, R., Arns, M., Jongsma, M. L. A., & Kessels, R. P. C. (2014). P300 development across the lifespan: A systematic review and meta-analysis. *PLoS One, 9*, e87347.

Dutta, A. (2015). Bidirectional interactions between neuronal and hemodynamic responses to transcranial direct current stimulation (tDCS): Challenges for brain-state dependent tDCS. *Frontiers in Systems Neuroscience, 9*, 1–7.

Dutta, A., Jacob, A., Chowdhury, S. R., Das, A., & Nitsche, M. A. (2015). EEG-NIRS based assessment of neurovascular coupling during anodal transcranial direct current stimulation – a stroke case series. *Journal of Medical Systems, 39*, 205.

Edwards, G., & Weston, A. H. (1993). The pharmacology of ATP-sensitive potassium channels. *Annual Review of Pharmacology and Toxicology, 33*, 597–637.

Faehling, F., & Plewnia, C. (2016). Controlling the emotional bias: Performance, late positive potentials, and the effect of anodal transcranial direct current stimulation (tDCS). *Frontiers in Cellular Neuroscience, 10*, 159.

Fang, Q. (2010). Mesh-based Monte Carlo method using fast ray-tracing in Plücker coordinates. *Biomedical Optics Express, 1*, 165–175.

Fantini, S. (2014). Dynamic model for the tissue concentration and oxygen saturation of hemoglobin in relation to blood volume, flow velocity, and oxygen consumption: Implications for functional neuroimaging and coherent hemodynamics spectroscopy (CHS). *NeuroImage, 85*(Pt 1), 202–221.

Faria, P., Fregni, F., Sebastião, F., Dias, A. I., & Leal, A. (2012). Feasibility of focal transcranial DC polarization with simultaneous EEG recording: Preliminary assessment in healthy subjects and human epilepsy. *Epilepsy & Behavior, 25*, 417–425.

Fernández-Corazza, M., Turovets, S., Luu, P., Anderson, E., & Tucker, D. (2016). Transcranial electrical neuromodulation based on the reciprocity principle. *Frontiers in Psychiatry, 7*, 87.

Filippini, N., MacIntosh, B. J., Hough, M. G., Goodwin, G. M., Frisoni, G. B., Smith, S. M., … Mackay, C. E. (2009). Distinct patterns of brain activity in young carriers of the APOE-epsilon4 allele. *Proceedings of the National Academy of Sciences of the United States of America, 106*, 7209–7214.

Fischl, B. (2012). FreeSurfer. *NeuroImage, 62*, 774–781.

Fornito, A., Zalesky, A., & Breakspear, M. (2013). Graph analysis of the human connectome: Promise, progress, and pitfalls. *NeuroImage, 80*, 426–444.

Fox, M. D., & Raichle, M. E. (2007). Spontaneous fluctuations in brain activity observed with functional magnetic resonance imaging. *Nature Reviews. Neuroscience, 8*, 700–711.

Giordano, J., Bikson, M., Kappenman, E. S., Clark, V. P., Coslett, H. B., Hamblin, M. R., … Calabrese, E. (2017). Mechanisms and effects of transcranial direct current stimulation. *Dose Response, 15*, 1559325816685467.

Girouard, H., & Iadecola, C. (2006). Neurovascular coupling in the normal brain and in hypertension, stroke, and Alzheimer disease. *Journal of Applied Physiology, 100*, 328–335.

Goncharova, I. I., McFarland, D. J., Vaughan, T. M., & Wolpaw, J. R. (2003). EMG contamination of EEG: Spectral and topographical characteristics. *Clinical Neurophysiology, 114*, 1580–1593.

Greischar, L. L., Burghy, C. A., Van Reekum, C. M., Jackson, D. C., Pizzagalli, D. A., Mueller, C., & Davidson, R. J. (2004). Effects of electrode density and electrolyte spreading in dense array electroencephalographic recording. *Clinical Neurophysiology, 115*, 710–720.

Guhathakurta, D., & Dutta, A. (2016). Computational pipeline for NIRS-EEG joint imaging of tDCS-evoked cerebral responses-an application in ischemic stroke. *Frontiers in Neuroscience, 10*, 261.

Hahn, C., Rice, J., Macuff, S., Minhas, P., Rahman, A., & Bikson, M. (2013). Methods for extra-low voltage transcranial direct current stimulation: Current and time dependent impedance decreases. *Clinical Neurophysiology, 124*, 551–556.

Hamel, E. (2006). Perivascular nerves and the regulation of cerebrovascular tone. *Journal of Applied Physiology, 100*, 1059–1064.

Helfrich, R. F., Knepper, H., Nolte, G., Strüber, D., Rach, S., Herrmann, C. S., … Engel, A. K. (2014). Selective modulation of interhemispheric functional connectivity by HD-tACS shapes perception. *PLoS Biology, 12*, e1002031.

Hess, G., Aizenman, C. D., & Donoghue, J. P. (1996). Conditions for the induction of long-term potentiation in layer II/III horizontal connections of the rat motor cortex. *Journal of Neurophysiology, 75*, 1765–1778.

Holland, R., Leff, A. P., Josephs, O., Galea, J. M., Desikan, M., Price, C. J., … Crinion, J. (2011). Speech facilitation by left inferior frontal cortex stimulation. *Current Biology, 21*, 1403–1407.

Holmes, C. J., Hoge, R., Collins, L., Woods, R., Toga, A. W., & Evans, A. C. (2015). Enhancement of MR images using registration for signal averaging. *Journal of Computer Assisted Tomography, 22*, 324–333.

Huneau, C., Benali, H., & Chabriat, H. (2015). Investigating human neurovascular coupling using functional neuroimaging: A critical review of dynamic models. *Frontiers in Neuroscience, 9*, 467.

Hunter, M. A., Coffman, B. A., Gasparovic, C., Calhoun, V. D., Trumbo, M. C., & Clark, V. P. (2015). Baseline effects of transcranial direct current stimulation on glutamatergic neurotransmission and large-scale network connectivity. *Brain Research, 1594*, 92–107.

Hunter, M. A., Coffman, B. A., Trumbo, M. C., & Clark, V. P. (2013). Tracking the neuroplastic changes associated with transcranial direct current stimulation: A push for multimodal imaging. *Frontiers in Human Neuroscience, 7*, 495.

Iwasaki, M., Kellinghaus, C., Alexopoulos, A. V., Burgess, R. C., Kumar, A. N., Han, Y. H., … Leigh, R. J. (2005). Effects of eyelid closure, blinks, and eye movements on the electroencephalogram. *Clinical Neurophysiology, 116*, 878–885.

Jasper, H. H. (1958). Report of the committee on methods of clinical examination in electroencephalography. *Electroencephalography and Clinical Neurophysiology. Supplement, 10*, 370–375.

Jenkinson, M., Beckmann, C. F., Behrens, T. E. J., Woolrich, M. W., & Smith, S. M. (2012). FSL. *NeuroImage, 62*, 782–790.

Jindal, U., Sood, M., Dutta, A., & Chowdhury, S. R. (2015). Development of point of care testing device for neurovascular coupling from simultaneous recording of EEG and NIRS during anodal transcranial direct current stimulation. *IEEE Journal of Translational Engineering in Health and Medicine, 3*, 1–12.

Johansen-Berg, H. (2013). Human connectomics – What will the future demand? *NeuroImage, 80*, 541–544.

Jolivet, R., Coggan, J. S., Allaman, I., & Magistretti, P. J. (2015). Multi-timescale modeling of activity-dependent metabolic coupling in the neuron-glia-vasculature ensemble. *PLoS Computational Biology, 11*, e1004036.

Kim, S., Stephenson, M. C., Morris, P. G., & Jackson, S. R. (2014). TDCS-induced alterations in GABA concentration within primary motor cortex predict motor learning and motor memory: A 7T magnetic resonance spectroscopy study. *NeuroImage, 99*, 237–243.

Kirilina, E., Jelzow, A., Heine, A., Niessing, M., Wabnitz, H., Brühl, R., … Tachtsidis, I. (2012). The physiological origin of task-evoked systemic artefacts in functional near infrared spectroscopy. *NeuroImage, 61*, 70–81.

Kitazono, T., Faraci, F. M., Taguchi, H., & Heistad, D. D. (1995). Role of potassium channels in cerebral blood vessels. *Stroke, 26*, 1713–1723.

Klass, D. W. (1995). The continuing challenge of artifacts in the EEG. *The American Journal of EEG Technology, 35*, 239–269.

Komssi, S., Aronen, H. J., Huttunen, J., Kesäniemi, M., Soinne, L., Nikouline, V. V., … Ilmoniemi, R. J. (2002). Ipsi- and contralateral EEG reactions to transcranial magnetic stimulation. *Clinical Neurophysiology, 113*, 175–184.

Kwon, Y. H., Ko, M.-H., Ahn, S. H., Minhas, P., Paulus, W., Kuo, M. F., & Nitsche, M. A. (2008). Primary motor cortex activation by transcranial direct current stimulation in the human brain. *Neuroscience Letters, 435*, 56–59. S0304-3940(08)00180-8 [pii].

Lee, S., & Buchsbaum, M. S. (1987). Topographic mapping of EEG artifacts. *Clinical Electroencephalography, 18*, 61–67.

Lemke, C., Hess, A., Clare, S., Bachtiar, V., Stagg, C., Jezzard, P., & Emir, U. (2015). Two-voxel spectroscopy with dynamic B<inf>0</inf> shimming and flip angle adjustment at 7 T in the human motor cortex. *NMR in Biomedicine, 28*, 852–860.

Leybaert, L., Paemeleire, K., Strahonja, A., & Sanderson, M. J. (1998). Inositol-trisphosphate-dependent intercellular calcium signaling in and between astrocytes and endothelial cells. *Glia, 24*, 398–407.

Light, G. A., Williams, L. E., Minow, F., Sprock, J., Rissling, A., Sharp, R., Swerdlow, N. R., & Braff, D. L. (2010). Electroencephalography (EEG) and event-related potentials (ERPs) with human participants. *Current Protocols in Neuroscience, 52*, 6.25.1–6.25.24.

Lindenberg, R., Nachtigall, L., Meinzer, M., Sieg, M. M., & Flöel, A. (2013). Differential effects of dual and unihemispheric motor cortex stimulation in older adults. *The Journal of Neuroscience, 33*, 9176–9183.

List, J., Lesemann, A., Kübke, J. C., Külzow, N., Schreiber, S. J., & Flöel, A. (2015). Impact of tDCS on cerebral autoregulation in aging and in patients with cerebrovascular diseases. *Neurology, 84*, 626–628.

Logothetis, N. K. (2008). What we can do and what we cannot do with fMRI. *Nature, 453*, 869–878.

Luft, C. D. B., & Bhattacharya, J. (2015). Aroused with heart: Modulation of heartbeat evoked potential by arousal induction and its oscillatory correlates. *Scientific Reports, 5*, 15717.

Mancini, M., Pellicciari, M. C., Brignani, D., Mauri, P., De Marchis, C., Miniussi, C., & Conforto, S. (2015). Automatic artifact suppression in simultaneous tDCS-EEG using adaptive filtering. In: Proceedings of the Annual International Conference of the IEEE Engineering in Medicine and Biology Society, EMBS. pp. 2729–2732

Mangia, A. L., Pirini, M., & Cappello, A. (2014). Transcranial direct current stimulation and power spectral parameters: A tDCS/EEG co-registration study. *Frontiers in Human Neuroscience, 8*, 601.

Mathiisen, T. M., Lehre, K. P., Danbolt, N. C., & Ottersen, O. P. (2010). The perivascular astroglial sheath provides a complete covering of the brain microvessels: An electron microscopic 3D reconstruction. *Glia, 58*, 1094–1103.

Maudsley, A. A., Darkazanli, A., Alger, J. R., Hall, L. O., Schuff, N., Studholme, C., … Zhu, X. (2006). Comprehensive processing, display and analysis for in vivo MR spectroscopic imaging. *NMR in Biomedicine, 19*, 492–503.

Meinzer, M., Lindenberg, R., Sieg, M. M., Nachtigall, L., Ulm, L., & Flöel, A. (2014). Transcranial direct current stimulation of the primary motor cortex improves word-retrieval in older adults. *Frontiers in Aging Neuroscience, 6*, 253.

Minhas, P., Bansal, V., Patel, J., Ho, J. S., Diaz, J., Datta, A., & Bikson, M. (2010). Electrodes for high-definition transcutaneous DC stimulation for applications in drug delivery and electrotherapy, including tDCS. *Journal of Neuroscience Methods, 190*, 188–197.

Mintun, M. A., Vlassenko, A. G., Rundle, M. M., & Raichle, M. E. (2004). Increased lactate/pyruvate ratio augments blood flow in physiologically activated human brain. *Proceedings of the National Academy of Sciences of the United States of America, 101*, 659–664.

Monai, H., Ohkura, M., Tanaka, M., Oe, Y., Konno, A., Hirai, H., … Hirase, H. (2016). Calcium imaging reveals glial involvement in transcranial direct current stimulation-induced plasticity in mouse brain. *Nature Communications, 7*, 11100.

Mulligan, S. J., & MacVicar, B. A. (2004). Calcium transients in astrocyte endfeet cause cerebrovascular constrictions. *Nature, 431*, 195–199.

Muthalib, M., Besson, P., Rothwell, J., Ward, T., & Perrey, S. (2016). Effects of anodal high-definition transcranial direct current stimulation on bilateral sensorimotor cortex activation during sequential finger movements: An fnirs study. *Advances in Experimental Medicine and Biology, 876*, 351–359.

Muthalib, M., Ferrari, M., Quaresima, V., Kerr, G., & Perrey, S. (2017). Functional near-infrared spectroscopy to probe sensorimotor region activation during electrical stimulation-evoked movement. *Clinical Physiology and Functional Imaging.*

Nelson, M. T., Patlak, J. B., Worley, J. F., & Standen, N. B. (1990). Calcium channels, potassium channels, and voltage dependence of arterial smooth muscle tone. *The American Journal of Physiology, 259*, C3–C18.

Niazy, R. K., Beckmann, C. F., Iannetti, G. D., Brady, J. M., & Smith, S. M. (2005). Removal of FMRI environment artifacts from EEG data using optimal basis sets. *NeuroImage, 28*, 720–737.

Nitsche, M. A., & Paulus, W. (2000). Excitability changes induced in the human motor cortex by weak transcranial direct current stimulation. *The Journal of Physiology, 527*(Pt 3), 633–639.

Nitsche, M. A., Schauenburg, A., Lang, N., Liebetanz, D., Exner, C., Paulus, W., & Tergau, F. (2003). Facilitation of implicit motor learning by weak transcranial direct current stimulation of the primary motor cortex in the human. *Journal of Cognitive Neuroscience, 15*, 619–626.

Noetscher, G. M., Yanamadala, J., Makarov, S. N., & Pascual-Leone, A. (2014). Comparison of cephalic and extracephalic montages for transcranial direct current stimulation – A numerical study. *IEEE Transactions on Biomedical Engineering, 61*, 2488–2498.

Noury, N., Hipp, J. F., & Siegel, M. (2016). Physiological processes non-linearly affect electrophysiological recordings during transcranial electric stimulation. *NeuroImage, 140*, 99–109.

Obrig, H. (2014). NIRS in clinical neurology – A "promising" tool? *NeuroImage, 85*, 535–546.

Okamoto, M., Dan, H., Sakamoto, K., Takeo, K., Shimizu, K., Kohno, S., … Dan, I. (2004). Three-dimensional probabilistic anatomical cranio-cerebral correlation via the international 10-20 system oriented for transcranial functional brain mapping. *NeuroImage, 21*, 99–111.

Oomagari, K., Buisson, B., Dumuis, A., Bockaert, J., & Pin, J. P. (1991). Effect of glutamate and lonomycin on the release of arachidonic acid, prostaglandins and HETEs from cultured neurons and astrocytes. *The European Journal of Neuroscience, 3*, 928–939.

Parra, L. C., Spence, C. D., Gerson, A. D., & Sajda, P. (2005). Recipes for the linear analysis of EEG. *Neuroimage, 28*, 326–341

Paulson, O. B., & Newman, E. A. (1987). Does the release of potassium from astrocyte endfeet regulate cerebral blood flow? *Science, 237*, 896–898.

Picton, T. W., & Hillyard, S. A. (1972). Cephalic skin potentials in electroencephalography. *Electroencephalography and Clinical Neurophysiology, 33*, 419–424.

Pievani, M., de Haan, W., Wu, T., Seeley, W. W., & Frisoni, G. B. (2011). Functional network disruption in the degenerative dementias. *Lancet Neurology, 10*, 829–843.

Pievani, M., Filippini, N., Van Den Heuvel, M. P., Cappa, S. F., & Frisoni, G. B. (2014). Brain connectivity in neurodegenerative diseases – From phenotype to proteinopathy. *Nature Reviews. Neurology, 10*, 620–633.

Polanía, R., Nitsche, M. A., Korman, C., Batsikadze, G., & Paulus, W. (2012). The importance of timing in segregated theta phase-coupling for cognitive performance. *Current Biology, 22*, 1314–1318.

Polanía, R., Nitsche, M. A., & Paulus, W. (2011a). Modulating functional connectivity patterns and topological functional organization of the human brain with transcranial direct current stimulation. *Human Brain Mapping, 32*, 1236–1249.

Polanía, R., Paulus, W., Antal, A., & Nitsche, M. A. (2011b). Introducing graph theory to track for neuroplastic alterations in the resting human brain: A transcranial direct current stimulation study. *NeuroImage, 54*, 2287–2296.

Pulgar, V. M. (2015). Direct electric stimulation to increase cerebrovascular function. *Frontiers in Systems Neuroscience, 9*, 54.

Raichle, M. E., MacLeod, A. M., Snyder, A. Z., Powers, W. J., Gusnard, D. A., & Shulman, G. L. (2001). A default mode of brain function. *Proceedings of the National Academy of Sciences of the United States of America, 98*, 676–682.

Reis, J., Schambra, H. M., Cohen, L. G., Buch, E. R., Fritsch, B., Zarahn, E., … Krakauer, J. W. (2009). Noninvasive cortical stimulation enhances motor skill acquisition over multiple days through an effect on consolidation. *Proceedings of the National Academy of Sciences of the United States of America, 106*, 1590–1595.

Roy, A., Baxter, B., & He, B. (2014). High-definition transcranial direct current stimulation induces both acute and persistent changes in broadband cortical synchronization: A simultaneous tDCS-EEG study. *IEEE Transactions on Biomedical Engineering, 61*, 1967–1978.

Roy, C. S., & Sherrington, C. S. (1890). On the regulation of the blood-supply of the brain. *The Journal of Physiology, 11*, 85–158.17.

Rubin, D., & Daube, J. (2016). Adult EEG: Artifacts and the EEG. *Clinical Neurophysiology.* Oxford University Press.

Schestatsky, P., Simis, M., Freeman, R., Pascual-Leone, A., & Fregni, F. (2013). Non-invasive brain stimulation and the autonomic nervous system. *Clinical Neurophysiology, 124*, 1716–1728.

Schmitt, S. (2017). Artifacts resembling seizures. In *Continuous EEG monitoring* (pp. 153–171). Cham, Switzerland: Springer International Publishing.

Scholkmann, F., Kleiser, S., Metz, A. J., Zimmermann, R., Mata Pavia, J., Wolf, U., & Wolf, M. (2014). A review on continuous wave functional near-infrared spectroscopy and imaging instrumentation and methodology. *NeuroImage, 85*, 6–27.

Schroeder, P. A., Ehlis, A. C., Wolkenstein, L., Fallgatter, A. J., & Plewnia, C. (2015). Emotional distraction and bodily reaction: Modulation of autonomous responses by anodal tDCS to the prefrontal cortex. *Frontiers in Cellular Neuroscience, 9*, 482.

Sehm, B., Kipping, J., Schäfer, A., Villringer, A., & Ragert, P. (2013). A comparison between Uni- and bilateral tDCS effects on functional connectivity of the human motor cortex. *Frontiers in Human Neuroscience, 7*, 183.

Sehm, B., Schäfer, A., Kipping, J., Margulies, D., Conde, V., Taubert, M., … Ragert, P. (2012). Dynamic modulation of intrinsic functional connectivity by transcranial direct current stimulation. *Journal of Neurophysiology, 108*, 3253–3263.

Shackman, A. J., McMenamin, B. W., Slagter, H. A., Maxwell, J. S., Greischar, L. L., & Davidson, R. J. (2009). Electromyogenic artifacts and electroencephalographic inferences. *Brain Topography, 22*, 7–12.

Smith, S. M., Fox, P. T., Miller, K. L., Glahn, D. C., Fox, P. M., Mackay, C. E., … Beckmann, C. F. (2009). Correspondence of the brain's functional architecture during activation and rest. *Proceedings of the National Academy of Sciences, 106*, 13040–13045.

Snyder, A. Z., & Raichle, M. E. (2012). A brief history of the resting state: The Washington University perspective. *NeuroImage, 62*, 902–910.

Sood, M., Besson, P., Muthalib, M., Jindal, U., Perrey, S., Dutta, A., & Hayashibe, M. (2016). NIRS-EEG joint imaging during transcranial direct current stimulation: Online parameter estimation with an autoregressive model. *Journal of Neuroscience Methods, 274*, 71–80.

Sood, M., Jindal, U., Chowdhury, S. R., Das, A., Kondziella, D., & Dutta, A. (2015). Anterior temporal artery tap to identify systemic interference using short-separation NIRS measurements: A NIRS/EEG-tDCS study. Conf proc. *Annual International Conference of the IEEE Engineering in Medicine and Biology Society. IEEE Engineering in Medicine and Biology Society. Annual Conference, 2015*, 1239–1242.

Stagg, C. J., Bachtiar, V., & Johansen-Berg, H. (2011a). The role of GABA in human motor learning. *Current Biology, 21*, 480–484.

Stagg, C. J., Best, J. G., Stephenson, M. C., O'Shea, J., Wylezinska, M., Kincses, Z. T., … Johansen-Berg, H. (2009a). Polarity-sensitive modulation of cortical neurotransmitters by transcranial stimulation. *The Journal of Neuroscience, 29*, 5202–5206.

Stagg, C. J., Jayaram, G., Pastor, D., Kincses, Z. T., Matthews, P. M., & Johansen-Berg, H. (2011b). Polarity and timing-dependent effects of transcranial direct current stimulation in explicit motor learning. *Neuropsychologia, 49*, 800–804.

Stagg, C. J., Lin, R. L., Mezue, M., Segerdahl, A., Kong, Y., Xie, J., & Tracey, I. (2013). Widespread modulation of cerebral perfusion induced during and after transcranial direct current stimulation applied to the left dorsolateral prefrontal cortex. *The Journal of Neuroscience, 33*, 11425–11431.

Stagg, C. J., & Nitsche, M. A. (2011). Physiological basis of transcranial direct current stimulation. *The Neuroscientist, 17*, 37–53.

Stagg, C. J., O'Shea, J., Kincses, Z. T., Woolrich, M., Matthews, P. M., & Johansen-Berg, H. (2009b). Modulation of movement-associated cortical activation by transcranial direct current stimulation. *The European Journal of Neuroscience, 30*, 1412–1423.

Stagg, C. J., Wylezinska, M., Matthews, P. M., Johansen-Berg, H., Jezzard, P., Rothwell, J. C., & Bestmann, S. (2009c). Neurochemical effects of Theta burst stimulation as assessed by magnetic resonance spectroscopy. *Journal of Neurophysiology, 101*, 2872–2877.

Strangman, G. E., Li, Z., & Zhang, Q. (2013). Depth sensitivity and source-detector separations for near infrared spectroscopy based on the Colin27 brain template. *PLoS One, 8*, e66319.

Stucht, D., Danishad, K. A., Schulze, P., Godenschweger, F., Zaitsev, M., & Speck, O. (2015). Highest resolution in vivo human brain MRI using prospective motion correction. *PLoS One, 10*, e0133921.

Tachtsidis, I., & Scholkmann, F. (2016). False positives and false negatives in functional near-infrared spectroscopy: Issues, challenges, and the way forward. *Neurophotonics, 3*, 31405.

Takai, H., Tsubaki, A., Sugawara, K., Miyaguchi, S., Oyanagi, K., Matsumoto, T., … Yamamoto, N. (2016). Effect of transcranial direct current stimulation over the primary motor cortex

on cerebral blood flow: A time course study using near-infrared spectroscopy. *Advances in Experimental Medicine and Biology, 876*, 335–341.

Tassinary, L. G., Cacioppo, J. T., & Vanman, E. J. (2007). The skeletomotor system. In G. Berntson, J. T. Cacioppo, & L. G. Tassinary (Eds.), *Handbook of psychophysiology* (pp. 267–300). Cambridge: Cambridge University Press.

Tenke, C. E., & Kayser, J. (2001). A convenient method for detecting electrolyte bridges in multichannel electroencephalogram and event-related potential recordings. *Clinical Neurophysiology, 112*, 545–550.

Torricelli, A., Contini, D., Pifferi, A., Caffini, M., Re, R., Zucchelli, L., & Spinelli, L. (2014). Time domain functional NIRS imaging for human brain mapping. *NeuroImage, 85*, 28–50.

Trepel, C., & Racine, R. J. (1998). Long-term potentiation in the neocortex of the adult, freely moving rat. *Cerebral Cortex, 8*, 719–729.

Trepel, C., & Racine, R. J. (2000). GABAergic modulation of neocortical long-term potentiation in the freely moving rat. *Synapse, 35*, 120–128.

Tsytsarev, V., Hu, S., Yao, J., Maslov, K., Barbour, D. L., & Wang, L. V. (2011). Photoacoustic microscopy of microvascular responses to cortical electrical stimulation. *Journal of Biomedical Optics, 16*, 76002.

Tzourio-Mazoyer, N., Landeau, B., Papathanassiou, D., Crivello, F., Etard, O., Delcroix, N., … Joliot, M. (2002). Automated anatomical labeling of activations in SPM using a macroscopic anatomical parcellation of the MNI MRI single-subject brain. *NeuroImage, 15*, 273–289.

Vaishnavi, S. N., Vlassenko, A. G., Rundle, M. M., Snyder, A. Z., Mintun, M. A., & Raichle, M. E. (2010). Regional aerobic glycolysis in the human brain. *Proceedings of the National Academy of Sciences, 107*, 17757–17762.

Vandermeeren, Y., Jamart, J., & Ossemann, M. (2010). Effect of tDCS with an extracephalic reference electrode on cardio-respiratory and autonomic functions. *BMC Neuroscience, 11*, 38.

Vernieri, F., Assenza, G., Maggio, P., Tibuzzi, F., Zappasodi, F., Altamura, C., … Rossini, P. M. (2010). Cortical neuromodulation modifies cerebral vasomotor reactivity. *Stroke, 41*, 2087–2090.

Villamar, M. F., Volz, M. S., Bikson, M., Datta, A., Dasilva, A. F., & Fregni, F. (2013). Technique and considerations in the use of 4x1 ring high-definition transcranial direct current stimulation (HD-tDCS). *Journal of Visualized Experiments*, e50309.

Wachter, D., Wrede, A., Schulz-Schaeffer, W., Taghizadeh-Waghefi, A., Nitsche, M. A., Kutschenko, A., … Liebetanz, D. (2011). Transcranial direct current stimulation induces polarity-specific changes of cortical blood perfusion in the rat. *Experimental Neurology, 227*, 322–327.

Wagner, S., Lucka, F., Vorwerk, J., Herrmann, C. S., Nolte, G., Burger, M., & Wolters, C. H. (2016). Using reciprocity for relating the simulation of transcranial current stimulation to the EEG forward problem. *NeuroImage, 140*, 163–173.

Waterink, W., & van Boxtel, A. (1994). Facial and jaw-elevator EMG activity in relation to changes in performance level during a sustained information processing task. *Biological Psychology, 37*, 183–198.

Westmoreland, B. F. (1996). Periodic patterns in the EEG. *American Journal of Electroneurodiagnostic Technology, 36*, 1–17.

Whitham, E. M., Pope, K. J., Fitzgibbon, S. P., Lewis, T., Clark, C. R., Loveless, S., … Willoughby, J. O. (2007). Scalp electrical recording during paralysis: Quantitative evidence that EEG frequencies above 20 Hz are contaminated by EMG. *Clinical Neurophysiology, 118*, 1877–1888.

Willis, J., Nelson, A., Rice, J., & Black, F. W. (1993). The topography of muscle activity in quantitative EEG. *Clinical Electroencephalography, 24*, 123–126.

Windhoff, M., Opitz, A., & Thielscher, A. (2013). Electric field calculations in brain stimulation based on finite elements: An optimized processing pipeline for the generation and usage of accurate individual head models. *Human Brain Mapping, 34*, 923–935.

Woods, A. J., Antal, A., Bikson, M., Boggio, P. S., Brunoni, A. R., Celnik, P., … Nitsche, M. A. (2016). A technical guide to tDCS, and related non-invasive brain stimulation tools. *Clinical Neurophysiology, 127*, 1031–1048.

Woods, A. J., Hamilton, R. H., Kranjec, A., Minhaus, P., Bikson, M., Yu, J., & Chatterjee, A. (2014). Space, time, and causality in the human brain. *NeuroImage, 92*, 285–297.

Yang, J., Ruchti, E., Petit, J.-M., Jourdain, P., Grenningloh, G., Allaman, I., & Magistretti, P. J. (2014). Lactate promotes plasticity gene expression by potentiating NMDA signaling in neurons. *Proceedings of the National Academy of Sciences of the United States of America, 111*, 12228–12233.

Zheng, X., Alsop, D. C., & Schlaug, G. (2011). Effects of transcranial direct current stimulation (tDCS) on human regional cerebral blood flow. *NeuroImage, 58*, 26–33.

Zuchowski, M. L., Timmann, D., & Gerwig, M. (2014). Acquisition of conditioned eyeblink responses is modulated by cerebellar tDCS. *Brain Stimulation, 7*, 525–531.